Open Access

*Journal of Energy and Power Technology*

LIDSEN Publishing Inc.

Original Research

# Harvesting Indoor Light for Electricity Recovery Using Semitransparent CdTe Solar Cells for Energy Efficient Buildings

Anudeep Katepalli [1], Anton Harfmann [2], Mathias Bonmarin [3], John Krupczak [4], Donglu Shi [1, *]

1. Materials Science and Engineering Program, Department of Mechanical and Materials Engineering, College of Engineering and Applied Science, University of Cincinnati, Cincinnati, OH 45221, USA; E-Mails: katepaap@mail.uc.edu; shid@ucmail.uc.edu
2. College of Design, Architecture, Art and Planning, University of Cincinnati, Cincinnati, OH 45221, USA; E-Mail: harfmaac@ucmail.uc.edu
3. School of Engineering, Zurich University of Applied Sciences, 8400 Winterthur, Switzerland; E-Mail: bmat@zhaw.ch
4. Department of Engineering, Hope College, Holland, MI 49423, USA; E-Mail: krupczak@hope.edu

* **Correspondence:** Donglu Shi; E-Mail: shid@ucmail.uc.edu

**Academic Editor:** Erdem Cuce

*Journal of Energy and Power Technology*
2026, volume 8, issue 4
doi:10.21926/jept.2604019

**Received:** August 05, 2026
**Accepted:** October 18, 2026
**Published:** November 02, 2026

**Abstract**

This study presents a preliminary proof-of-concept demonstration exploring how indoor artificial lighting - specifically LED systems - can serve a dual function: providing illumination while enabling electricity generation through integration with semitransparent photovoltaic (PV) panels. Using cadmium telluride (CdTe) PV cells with varying visible light transmittance levels, we show that diffused indoor LED lighting can generate meaningful electrical output, even under relatively low light power densities. A multi-layer panel configuration further enhances power output, with cumulative power conversion efficiencies substantially exceeding those of individual panels. While the photovoltaic efficiencies remain lower than those of optimized outdoor solar systems operating under standard AM 1.5 conditions, the results demonstrate the feasibility of continuous indoor photon harvesting independent of weather variability. The experiments were conducted under controlled indoor LED illumination and are intended to establish a conceptual framework for integrating energy-

© 2026 by the author. This is an open access article distributed under the conditions of the Creative Commons by Attribution License, which permits unrestricted use, distribution, and reproduction in any medium or format, provided the original work is correctly cited.

harvesting systems within interior spaces - including walls, ceilings, and floors - as a pathway toward energy-neutral buildings. From a cost-benefit perspective, if 15% efficient PV panels were installed on 30% of the Willis Tower's usable interior surface area, yielding illustrative scenario-based annual electricity savings of approximately $0.81 million under baseline assumptions. These findings highlight the potential of transforming indoor lighting environments into distributed supplemental energy-generation systems supporting long-term building sustainability and reduced energy consumption.

**Keywords**
Indoor light harvesting; CdTe PV; spectral loss; transparent multi-panels; continuous electricity generation; energy-neutral building

## 1. Introduction

Photovoltaic (PV) solar cells have become increasingly popular and are extensively used across various applications because of their technical, environmental, and sustainability advantages [1-4]. However, the performance of outdoor photovoltaic systems depends strongly on available solar irradiance, which varies with weather conditions, seasonal changes, atmospheric attenuation, and day-night cycles. As a result, outdoor PV systems experience temporal fluctuations in electrical power generation. In contrast, indoor photovoltaic systems operating under controlled LED illumination can experience more stable and predictable photon exposure conditions. Despite the established efficiency of PV technology as a sustainable energy source, conventional photovoltaic deployment remains largely restricted to two-dimensional (2D) exterior surfaces such as rooftops and facades. One important application is building-integrated photovoltaics (BIPV), where building skins are utilized for solar harvesting. However, the limited roof-to-floor-area ratio in large multi-story buildings constrains the total available exterior harvesting area and often prevents sufficient energy generation to meet building-scale demand [5-9]. This challenge is particularly significant in densely populated urban environments and motivates the development of advanced photovoltaic technologies capable of harvesting diffuse and low-intensity indoor light sources.

In modern urban environments, high-rise buildings consume substantial electrical energy for indoor illumination, particularly during nighttime operation [10-16]. In many commercial and public infrastructures, indoor lighting systems remain active for extended periods to support occupancy, safety, navigation, architectural illumination, and operational requirements. As a result, substantial optical power is continuously distributed throughout interior spaces.

The concept explored in this work is based on indoor optical energy recovery and distributed photon utilization. Rather than treating indoor illumination solely as an energy-consuming process, the present study investigates whether a fraction of the emitted photon flux from electrically powered lighting systems can be partially recaptured using semitransparent photovoltaic (PV) structures integrated into interior architectural spaces. In this framework, the proposed system does not constitute net energy generation, but rather a supplemental optical energy recovery mechanism operating within existing lighting infrastructures.

Semitransparent photovoltaic panels integrated into walls, ceilings, windows, or suspended interior structures may enable partial recovery of incident indoor optical energy while maintaining architectural functionality and visible-light transmission. Because indoor illumination environments are spatially distributed and continuously active for long operational periods, they provide a unique platform for investigating distributed low-intensity photon harvesting within the built environment.

Indoor LED illumination has previously been investigated for low-light photovoltaic energy harvesting applications [17-20]. As illustrated schematically in Figure 1, semitransparent photovoltaic panels may be architecturally integrated into indoor and outdoor building structures to interact with incident optical fields generated by artificial lighting systems. Because photovoltaic response depends strongly on spectral matching between the illumination source and the absorber bandgap, selected LED wavelengths can influence the measured photovoltaic response of the CdTe devices.

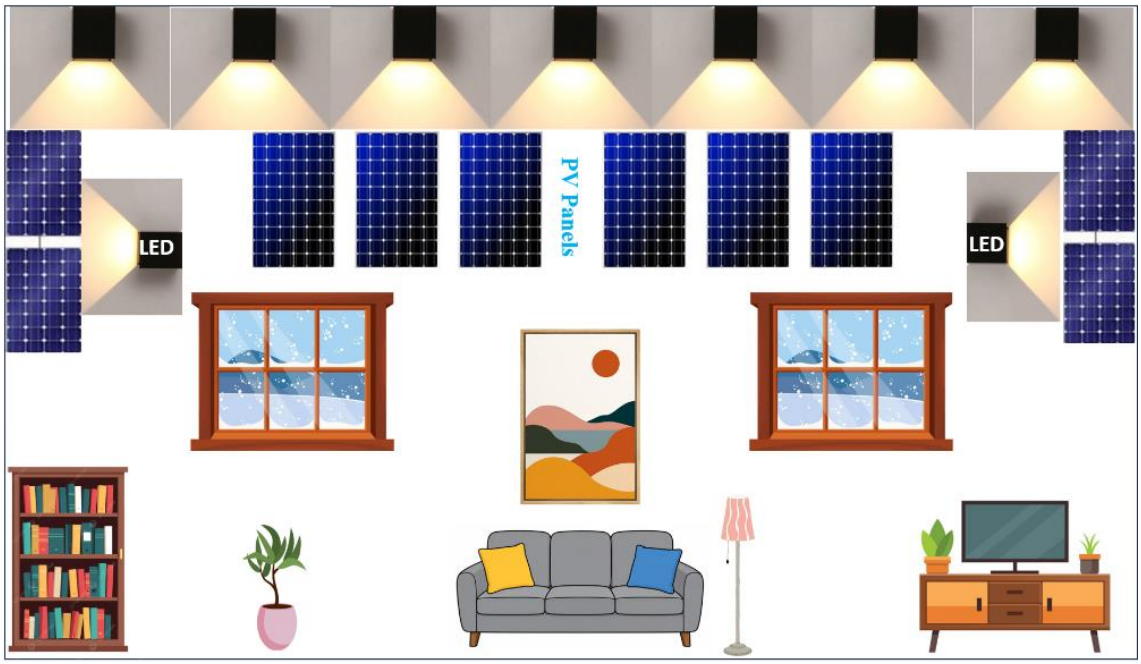



**Figure 1** Schematic illustration of the concept of wall-mounted photovoltaic panels designed to harvest diffused light emitted from indoor LED sources.

The objective of the present work is therefore not to demonstrate net energy production, but rather to experimentally evaluate the feasibility of partial optical energy recovery using semitransparent CdTe photovoltaic systems under controlled LED illumination conditions. In particular, the study investigates multilayer semitransparent photovoltaic configurations designed to enhance photon utilization through sequential transmission and absorption across multiple layers.

Outdoor photovoltaic systems operate under significantly higher irradiance conditions than indoor systems but are inherently dependent on solar availability and environmental variability. In contrast, indoor illumination environments provide controlled and temporally stable optical conditions that are useful for investigating low-intensity photovoltaic operation and photon-utilization strategies. Although the electrical power density available indoors is substantially lower than outdoor solar irradiance, continuously illuminated interior environments offer an opportunity

to study distributed optical energy recovery using semitransparent photovoltaic architectures integrated within building spaces.

Unlike conventional indoor photovoltaic studies focused primarily on single low-power energy-harvesting devices, the present work experimentally investigates multilayer semitransparent CdTe photovoltaic architectures under controlled wavelength-selective LED illumination, with emphasis on photon transmission through sequential photovoltaic layers and its implications for distributed indoor optical energy recovery within building-scale environments.

Indoor photovoltaic (PV) energy harvesting is fundamentally constrained by low light intensities, spectral mismatch between artificial lighting and solar cell absorption, limited deployment area, and non-uniform illumination. Typical indoor irradiance levels are orders of magnitude lower than direct sunlight, drastically reducing the photon flux available to PV devices and, consequently, their achievable power output. Moreover, artificial light sources such as light-emitting diodes (LEDs) exhibit relatively narrow emission spectra that often do not optimally overlap with the absorption profiles of conventional solar cells, leading to suboptimal conversion efficiency under indoor conditions.

Figure 1 provides a conceptual architectural schematic illustrating the integration of semitransparent photovoltaic panels within interior spaces. Detailed physical panel dimensions, quantitative electrical parameters, and structured light paths for the multilayer test configurations are detailed in subsequent data plots and experimental schematics.

To address these challenges, the present work employs semitransparent cadmium telluride (CdTe) solar cells in a vertically stacked, multilayer configuration. By stacking multiple thin CdTe panels along the vertical (z-axis) direction, the same footprint can be used to harvest light sequentially, effectively extending the active light-collection volume into the third dimension. Transmitted photons that are not absorbed by upper layers can be captured by lower layers, enabling improved overall system power conversion efficiency (PCE) without increasing the surface area required for installation. The primary objective of this research is to determine whether indoor LED lighting can generate sufficient electricity using semitransparent CdTe PV solar cells. Given that power conversion efficiency (PCE) is highly dependent on photon wavelength, we employed LEDs spanning a broad spectral range - from ultraviolet (UV) to near - infrared (NIR). This approach allows us to identify optimal LED - PV combinations for effective photon recycling. The findings can inform architectural and lighting design strategies to maximize indoor energy harvesting, particularly in urban settings where electricity demand is constant and reliability is critical. Photon recycling using indoor lighting presents a promising solution to the intermittency of traditional solar systems, which are limited by nightfall and cloudy weather. In this context, indoor LEDs not only serve functional and aesthetic roles within buildings but also contribute to diversified, distributed energy generation. Such systems offer more stable power output and enhance the resilience of renewable energy infrastructures.

In our study, we investigate the spectral response of semitransparent cadmium telluride (CdTe) solar panels under illumination from LEDs with different wavelengths. It is well known that the spectral response of PV cells is highly sensitive to photon energy. For silicon - based PVs, maximum spectral response occurs near the bandgap energy ($E_g \approx 1.1$ eV), but significant spectral losses occur in both the ultraviolet and infrared regions. Unlike solar irradiance, which spans a broad spectrum, LEDs typically emit within narrow wavelength bands. If this emission matches the PV's bandgap, energy conversion efficiency can be significantly enhanced.

Our investigation focuses on characterizing the wavelength-dependent PCE of semi-transparent CdTe PVs under controlled LED illumination spanning the ultraviolet (UV) to near-infrared (NIR) range. In parallel, we experimentally explore multilayer stacking with varying average visible transmittance (AVT), demonstrating how photon harvesting can enhance system-level efficiency relative to a single-panel configuration.

The novelty of this research lies not merely in reporting indoor PV operation, but in reconceptualizing indoor photovoltaic harvesting as a system-level, three-dimensional energy-harvesting strategy. Prior indoor PV studies have largely focused on single-layer devices optimized for low-power Internet-of-Things (IoT) applications, using materials such as GaAs, GaInP, perovskites, or dye-sensitized solar cells, typically evaluated under fixed white LED or fluorescent spectra. In contrast, semitransparent CdTe modules have been primarily investigated for outdoor building-integrated photovoltaics (BIPV) and day-lighting, with limited quantitative study under indoor artificial lighting and virtually no experimental work addressing multilayer system-level efficiency enhancement.

This study distinguishes itself by (i) providing a systematic wavelength-dependent evaluation of semitransparent CdTe PV performance under LED illumination from UV to NIR, explicitly revealing spectral matching effects and identifying NIR illumination as yielding higher PCE than natural sunlight for CdTe; (ii) introducing and experimentally validating a multilayer, 3D stacking architecture for indoor PV harvesting that demonstrates photon utilization; and (iii) framing indoor PV as a photon-recycling strategy for energy-neutral buildings, supported by quantitative scalability and techno-economic considerations. To the best of our knowledge, this is the first study to integrate spectral optimization, multilayer CdTe stacking, and continuous indoor LED illumination into a unified experimental framework.

Semitransparent CdTe modules were selected for three reasons combining practical and scientific considerations. First, these modules were already available in our laboratory from prior photovoltaic investigations, allowing controlled indoor LED experiments with well-characterized devices and reproducible electrical performance. Second, their semi-transparency, with average visible transmittance (AVT) ranging from 40% to 80%, makes them suitable for multilayer stacking experiments, as the transmitted fraction enables photon harvesting by downstream layers. Third, CdTe is a direct-bandgap semiconductor with strong absorption extending into the near-infrared, permitting examination of wave-length-dependent photovoltaic response under LEDs covering UV to NIR regions. We emphasize that CdTe serves primarily as a stable proof-of-concept platform for studying indoor photon harvesting and multilayer stacking; we do not claim it is necessarily the optimal material for indoor photovoltaics.

Crystalline silicon, dominant in outdoor solar energy conversion, has comparatively weak absorption per unit thickness and is less suited to semitransparent multilayer stacking without substantial thickness or structural modification. Organic and hal-ide-perovskite photovoltaics can be tuned for strong low-intensity indoor performance, but long-term stability and large-area encapsulation remain significant challenges. Amorphous silicon offers improved absorption relative to crystalline silicon but generally exhibits lower carrier mobility and efficiency. Within this context, CdTe provides an established module-scale platform with proven durability, making it a practical baseline for evaluating the architectural concept of semitransparent multilayer photon harvesting un-der indoor illumination.

It is essential to emphasize from a thermodynamic perspective that harvesting light from electrically powered indoor LED systems does not constitute net energy generation. Instead, the configuration operates strictly as an intra-system optical energy recovery mechanism. Governed by the second law of thermodynamics, the complete energy conversion chain entails initial electrical input converted to optical energy via LED wall-plug efficiency ($\eta_{wp}$ ≈ 25-40%), followed by optical-to-electrical conversion through photovoltaic panels (PCE ≈ 10-15%). This multiplicative loss chain yields an overall round-trip efficiency of approximately 2.5-6%. Consequently, the photovoltaic output captured from indoor lighting represents a partial recapture of otherwise dissipated optical energy rather than an independent source of primary power. Furthermore, to avoid confusion with internal radiative recombination and photon reabsorption phenomena traditionally studied in photovoltaic physics, the mechanism described herein is designated strictly as 'optical energy recovery' rather than 'photon recycling'.

While direct monochromatic external quantum efficiency (EQE) characterization is precluded by the encapsulated nature of the commercial modules evaluated here, this study focuses on system-level multi-wavelength indoor characterization to assess aggregate optical energy recovery. While our previous work [21] established foundational proof-of-concept multi-panel stacking for outdoor CdTe modules, the present study significantly extends this framework by introducing: (i) systematic multi-wavelength indoor LED spectral sweeps across discrete optical bands; (ii) a direct performance comparison between side-by-side parallel arrangements and tight 3D vertical photon-harvesting stacks; and (iii) an updated, consolidated techno-economic analysis detailing building-scale integration and sensitivity payback horizons.

## 2. Experimental Procedure

Figure 2 shows the photographs of the CdTe PVs with different AVTs. We utilized five commercial CdTe solar panels (Solar First Technology Co) with dimensions of 150 × 150 $mm^2$ for I-V measurements under LEDs of different wavelengths [21]. These panels had varying average visible transmittance (AVT) values of 80%, 70%, 60%, 50%, and 40%, respectively (Figure 2). The SourceMeter instrument was connected to each Device Under Test (DUT), which in this case were the CdTe panels. The sourcing mode was configured as a voltage source to enable voltage sweeping for obtaining I-V curves. The voltage sweep range started from 0V and concluded at 20 V, with the SourceMeter measuring the current flowing through the DUT at each voltage step. A total of 400 steps were performed throughout the experiment. Throughout this study, panel stacking arrangements are designated by their transparency order relative to the incident light source: ascending order refers to positioning the lowest average visible transmittance (AVT) panel (40%) closest to the light source, followed sequentially by higher AVT panels (50%, 60%, 70%, and 80%) underneath; conversely, descending order refers to placing the highest AVT panel (80%) on top, followed sequentially by lower AVT panels down to 40% at the bottom.

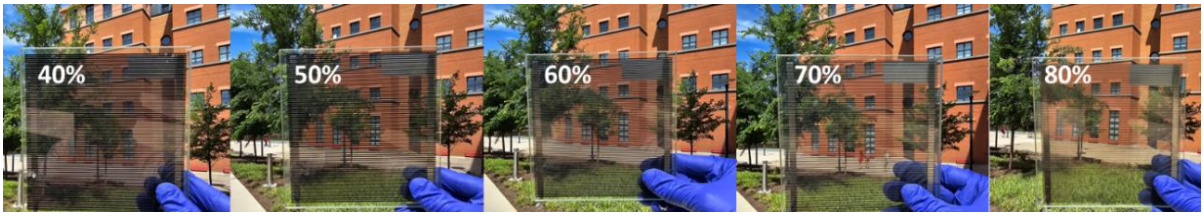



**Figure 2** CdTe solar panels with their average visible transmittance (AVT) indicated.

The CdTe devices used in this study are commercially manufactured, fully encapsulated semitransparent modules. As a result, destructive or invasive materials characterization-such as XRD, SEM, electroluminescence, or photoluminescence - was not performed, since disassembly could damage the devices and compromise manufacturer specifications. Detailed layer-stack information is typically proprietary for commercial modules; accordingly, this work focuses on system-level electrical response under controlled indoor LED illumination and multilayer stacking configurations, for which current-voltage (I-V) characterization under defined spectral and irradiance conditions provides the most relevant metric.

External quantum efficiency (EQE) measurements were likewise not conducted. For sealed commercial modules, EQE characterization requires monochromatic illumination and optical access to the active layers, which is not possible without destructive modification. Instead, wavelength-dependent behavior was assessed through full I-V measurements under LEDs with defined spectral ranges at controlled irradiance, offering a practical system-level proxy for spectral response under indoor conditions. While the use of five broad LED emission bands provides practical system-level insight into indoor performance under realistic lighting conditions, it represents a coarse spectral resolution compared to conventional monochromatic external quantum efficiency (EQE) measurements. Because the test devices are encapsulated commercial modules, direct EQE characterization was not feasible without destructive de-encapsulation. Consequently, the spectral matching analysis serves as an operational system-level proxy rather than a fine-grained quantum efficiency profile; future work will incorporate non-destructive narrow-band optical filtering to achieve higher spectral granularity.

The I-V measurements were carried out using 10 W BlueX LEDs (Manufacturer: BlueX Bulbs) of different colors (Figure 3). These are purple light (380 nm-435 nm), green light (495 nm-570 nm), orange light (585 nm-620 nm), and red light (630 nm-750 nm). An 86 W IR LED was also used with a wavelength range of 770 nm-850 nm (Figure 3e). As shown in Figure 3a, four LEDs were positioned above the CdTe PV panel at various distances. The distances between the LED bulbs and the CdTe PV panel were adjusted to maintain a consistent light power density of 30 mW/cm$^2$ across the CdTe panel for all I-V curve measurements. The I-V curves were experimentally obtained to calculate key parameters such as Open - Circuit Voltage ($V_{OC}$), Short - Circuit Current ($I_{SC}$), Maximum Power ($P_{MAX}$), Fill Factor (FF), and Power Conversion Efficiency (PCE). It should be noted that not all data points from the voltage steps were utilized for analysis; only the data within the range from $I_{SC}$ to $V_{OC}$ were considered. For plotting purposes, the absolute values of the cur-rent data points between $I_{SC}$ and $V_{OC}$ were used.

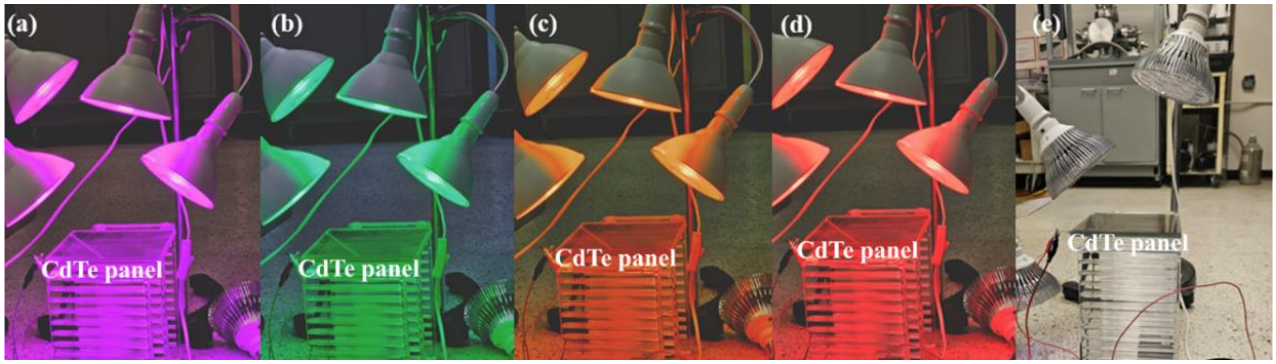



**Figure 3** Photographs of I-V measurement set up: (a) purple lights, (b) green lights, (c) orange lights, (d) red lights, and (e) IR lights.

Because the emission spectra of the LEDs used in this study are narrow and well de-fined by the manufacturer, no independent spectral calibration was performed. Instead, the experimental emphasis was placed on precise control and reproducibility of the incident light intensity at the photovoltaic (PV) surface. A calibrated optical power meter was used to measure the irradiance directly at the CdTe panel surface, and the LED-to-panel distance was adjusted iteratively until a uniform power density of 30 mW/cm$^2$ was achieved for single-panel measurements and 25 mW/cm$^2$ for multilayer configurations.

To account for spatial nonuniformity inherent to LED illumination, irradiance was measured at multiple locations across the active area of the PV panel, and the setup was adjusted to minimize variations. For each LED wavelength condition, ten independent current-voltage (I-V) measurements were performed under identical experimental conditions. Although the reported results are not statistical averages, repeated measurements consistently produced nearly identical I-V curves and extracted photovoltaic parameters, indicating high measurement repeatability and stability of the setup. To quantify spatial non-uniformity, optical power density measurements across multiple points of the 150 × 150 mm$^2$ panel surface indicated a deviation of approximately ±12% from the mean target irradiance. While localized intensity gradients can induce minor variations in regional diode performance and series resistance effects, the integrated electrical response reflects the aggregate system behavior under realistic diffuse indoor lighting.

Measurement uncertainty was minimal for several reasons. First, the CdTe panels used in this work have relatively low peak power output (approximately 1.2 W under full sunlight), ensuring that all measurements were conducted well within the linear and high-resolution operating range of both the SourceMeter and the optical power meter. Second, all experiments were carried out in a controlled indoor environment with negligible ambient light and minimal temperature variation, further reducing systematic and random errors. Taken together, these procedures ensure that the reported performance trends are reproducible and that experimental uncertainties do not influence the conclusions of this study. All reported current-voltage (I-V) parameters and power conversion efficiency (PCE) values represent the arithmetic mean of ten independent experimental measurements conducted under identical conditions. Standard deviations across trials were consistently within ±2% of the mean values, demonstrating high experimental reproducibility.

## 3. Results

### *3.1 I-V Curves of CdTe Solar Panels Under Natural Sunlight*

Figure 4 presents the I-V curves obtained from the CdTe solar panels under natural sunlight in open air, with the corresponding I-V parameters summarized in Table 1 [22]. As illustrated, each CdTe panel's I-V curve (Figure 4a) and output power (Figure 4b) correlate with their AVT values; specifically, panels with lower AVTs exhibit higher PCEs. Consequently, the panel with the lowest AVT (40%) achieved the highest PCE of 8.6% (Table 1). All CdTe panels demonstrated PCE values consistent with their AVTs, aligning with the data sheets provided by the manufacturer. The light power density under natural sunlight was measured at 55.4 mW/cm$^2$. These data will be used to compare with the I-V curves obtained under LED illumination.

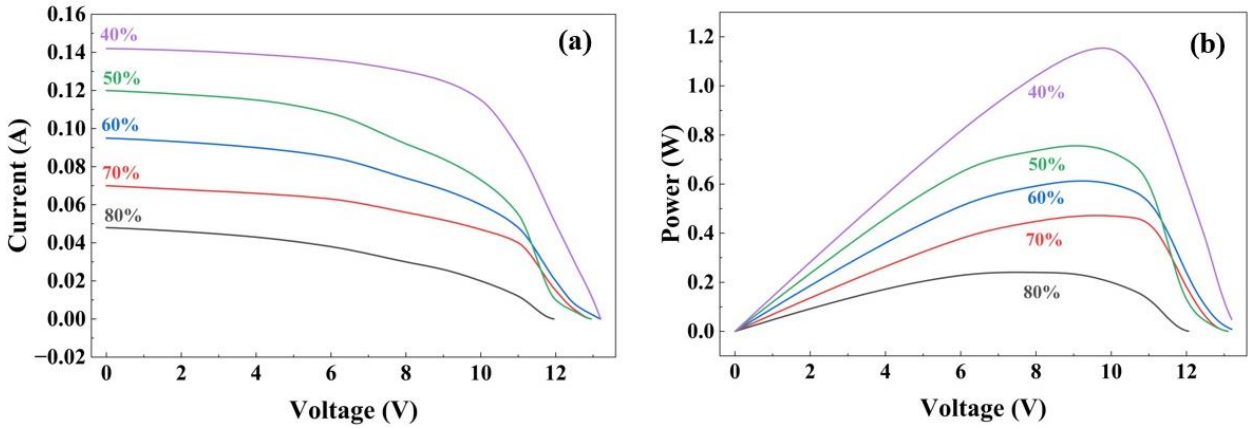



**Figure 4** (a) I-V curves and (b) output power of CdTe solar panels with different transparencies [21].

**Table 1** I-V curve parameters of the CdTe solar panels under natural sunlight [21].

| Solar Panel AVT | $V_{OC}$ (V) | $I_{SC}$ (A) | $P_{MAX}$ (W) | FF | PCE | Light Power Density (mW/cm$^2$) |
|---|---|---|---|---|---|---|
| 40% | 12.732 | 0.141 | 1.072 | 0.594 | 8.6% | 55.4 |
| 50% | 12.130 | 0.119 | 0.723 | 0.500 | 5.8% | 55.4 |
| 60% | 12.732 | 0.095 | 0.553 | 0.456 | 4.4% | 55.4 |
| 70% | 12.431 | 0.070 | 0.466 | 0.534 | 3.7% | 55.4 |
| 80% | 11.378 | 0.048 | 0.242 | 0.443 | 1.9% | 55.4 |

### *3.2 I-V Curves of CdTe Solar Panels Under LEDs*

The I-V curves of CdTe solar panels are presented in Figure 5 with different AVTs under LEDs of various wavelengths: (a) purple (380 nm-435 nm), (b) green (495 nm-570 nm), (c) orange (585 nm-620 nm), and (d) red (630 nm-750 nm). Consistent with the results under natural sunlight, the I-V curves indicate that panels with higher AVTs exhibit lower PCEs, and vice versa. The parameters for these I-V curves are detailed in Tables 2-5. The data reveal that PCE values obtained from purple light (the highest being 4.8% for 40% AVT, Table 2) are slightly higher than those from orange light (the highest being 3.3% for 40% AVT, Table 3). Green light results in the lowest PCE, with a maximum of 2% for 40% AVT (Table 4). Notably, despite maintaining a constant light power density of 30

mW/cm$^2$ for all measurements, PCE significantly increases under red light (630 nm-750 nm), with the highest PCE for the 40% AVT panel reaching 4.6% (Table 5).

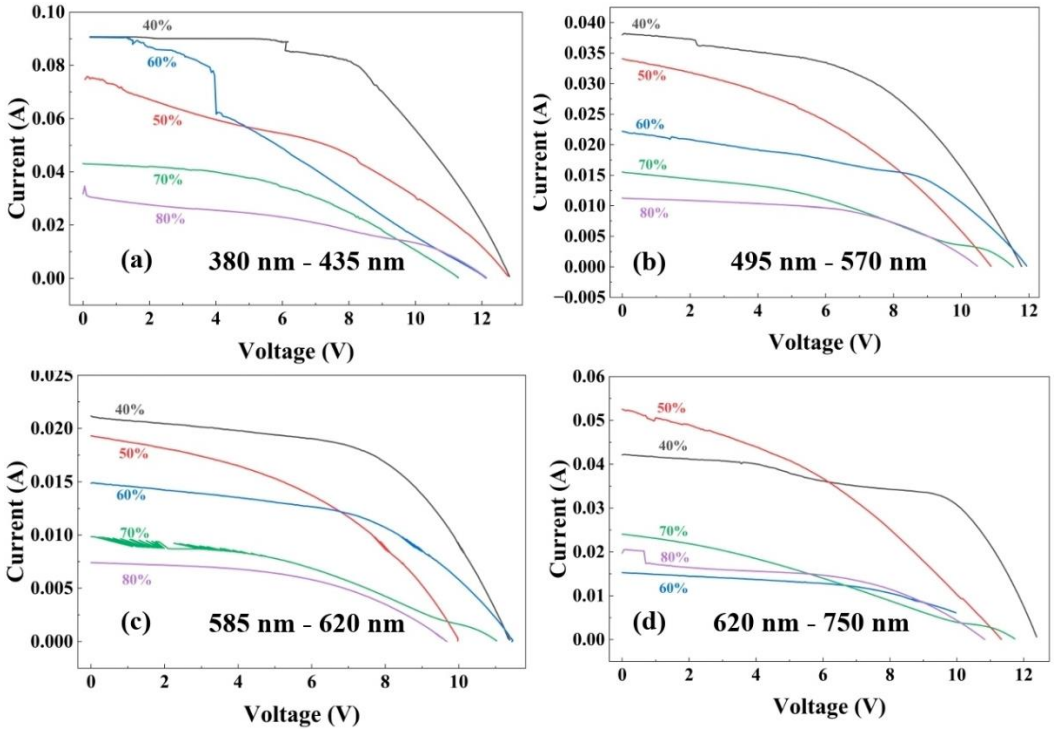



**Figure 5** I-V curves of the CdTe solar panels of different AVTs as indicated under LEDs of different wavelengths (a) purple: 380 nm-435 nm, (b) green: 495 nm-570 nm, (c) orange: 585 nm-620 nm, and (d) red: 630 nm-750 nm.

**Table 2** The I-V curve parameters of the CdTe solar panels under purple light (380 nm-435 nm).

| Solar Panel AVT | $V_{OC}$ (V) | $I_{SC}$ (A) | $P_{MAX}$ (W) | FF | PCE | Light Power Density (mW/cm$^2$) |
|---|---|---|---|---|---|---|
| 40% | 12.181 | 0.059 | 0.334 | 0.464 | 4.9% | 30 |
| 50% | 11.278 | 0.053 | 0.227 | 0.379 | 3.3% | 30 |
| 60% | 12.187 | 0.032 | 0.195 | 0.500 | 2.8% | 30 |
| 70% | 11.830 | 0.023 | 0.094 | 0.345 | 1.3% | 30 |
| 80% | 10.977 | 0.019 | 0.096 | 0.460 | 1.4% | 30 |

**Table 3** The I-V curve parameters of the CdTe solar panels under orange light (585 nm-620 nm).

| Solar Panel AVT | $V_{OC}$ (V) | $I_{SC}$ (A) | $P_{MAX}$ (W) | FF | PCE | Light Power Density (mW/cm$^2$) |
|---|---|---|---|---|---|---|
| 40% | 11.378 | 0.021 | 0.134 | 0.560 | 2% | 30 |
| 50% | 9.969 | 0.019 | 0.083 | 0.438 | 1.2% | 30 |
| 60% | 11.441 | 0.015 | 0.086 | 0.501 | 1.3% | 30 |
| 70% | 11.027 | 0.009 | 0.041 | 0.413 | 0.6% | 30 |
| 80% | 9.674 | 0.007 | 0.035 | 0.516 | 0.5% | 30 |

**Table 4** The I-V curve parameters of the CdTe solar panels under green light (495 nm-570 nm).

| Solar Panel AVT | $V_{OC}$ (V) | $I_{SC}$ (A) | $P_{MAX}$ (W) | FF | PCE | Light Power Density (mW/cm$^2$) |
|---|---|---|---|---|---|---|
| 40% | 11.780 | 0.038 | 0.225 | 0.502 | 3.3% | 30 |
| 50% | 10.877 | 0.034 | 0.145 | 0.392 | 2.1% | 30 |
| 60% | 11.931 | 0.022 | 0.129 | 0.491 | 1.9% | 30 |
| 70% | 11.534 | 0.015 | 0.066 | 0.381 | 0.8% | 30 |
| 80% | 10.476 | 0.011 | 0.061 | 0.529 | 0.9% | 30 |

**Table 5** The I-V curve parameters of the CdTe solar panels under red light (630 nm-750 nm).

| Solar Panel AVT | $V_{OC}$ (V) | $I_{SC}$ (A) | $P_{MAX}$ (W) | FF | PCE | Light Power Density (mW/cm$^2$) |
|---|---|---|---|---|---|---|
| 40% | 12.381 | 0.042 | 0.312 | 0.599 | 4.6% | 30 |
| 50% | 11.330 | 0.052 | 0.222 | 0.376 | 3.3% | 30 |
| 60% | 9.975 | 0.015 | 0.085 | 0.568 | 1.3% | 30 |
| 70% | 11.730 | 0.024 | 0.084 | 0.298 | 1.2% | 30 |
| 80% | 10.83 | 0.019 | 0.094 | 0.456 | 1.4% | 30 |

As shown in Table 4, a fundamental trade-off exists between visible-light transparency and photovoltaic conversion efficiency in semitransparent photovoltaic systems. Increasing average visible transmittance (AVT) generally reduces the optical absorption within the active photovoltaic layer, thereby decreasing the number of absorbed photons available for electrical conversion. Consistent with this behavior, lower-AVT CdTe panels in the present study exhibited higher electrical output and PCE values, whereas higher-AVT panels preserved greater optical transparency at the expense of reduced photovoltaic response. The multilayer semitransparent configuration investigated here therefore represents an approach for partially redistributing photon absorption across sequential photovoltaic layers while maintaining partial visible-light transmission throughout the structure.

The bandgap of CdTe is 1.5 eV, corresponding to a wavelength of 826 nm [23-28]. To match this wavelength for enhanced photon recovery, we employed IR light within the range of 770 nm to 850 nm. In this wavelength range, the CdTe solar cell is expected to achieve its highest PCE. Figure 6 shows the I-V curves obtained under IR light, with all relevant parameters detailed in Table 6. As illustrated in Figure 6 and Table 6, the highest PCE of the 40% AVT solar cell reaches 9.8%, which surpasses the PCE obtained under natural sunlight (8.6%). It is important to note that the light power density of natural sunlight is 55.4 mW/cm$^2$, higher than that of LED (30 mW/cm$^2$). Despite the lower light power density, the CdTe cell with 40% AVT exhibits a higher PCE under IR LED irradiation.

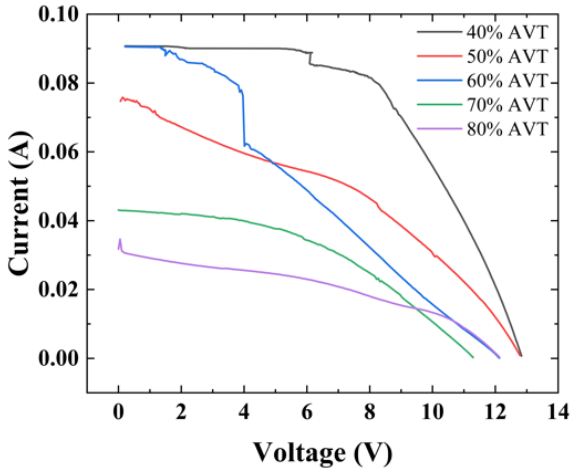



**Figure 6** I-V curves of the CdTe solar panels of different AVTs as indicated under LED with wavelength of 770 nm-850 nm.

**Table 6** The I-V curve parameters of the CdTe solar panels under lights (770 nm-850 nm).

| Solar Panel AVT | $V_{OC}$ (V) | $I_{SC}$ (A) | $P_{MAX}$ (W) | FF | PCE | Light Power Density (mW/cm$^2$) |
|---|---|---|---|---|---|---|
| 40% | 12.832 | 0.090 | 0.660 | 0.571 | 9.8% | 30 |
| 50% | 12.782 | 0.074 | 0.372 | 0.393 | 5.5% | 30 |
| 60% | 12.131 | 0.090 | 0.302 | 0.276 | 4.5% | 30 |
| 70% | 11.308 | 0.043 | 0.212 | 0.435 | 3.1% | 30 |
| 80% | 12.131 | 0.031 | 0.146 | 0.388 | 2.2% | 30 |

The PCE values of the CdTe solar panels with various AVTs plotted against the wavelength of LEDs as shown in Figure 7. As can be seen in this figure, PCEs tend to increase as the LED wavelength approaches 850 nm, corresponding to the bandgap of CdTe (1.5 eV). Notably, a minimum is observed in the visible range around 585 nm to 620 nm. The increase in PCE is particularly pronounced for the 40% AVT panel, while those with higher AVTs, such as 80%, exhibit minimal variations in PCE. It is important to highlight a significant difference between natural sunlight and LED light: while the former maintains uniform light power density, the latter's divergence results in non - uniformity. LEDs positioned at a distance from the CdTe panel cause a distribution of light power density across the PV panel surface, with the center receiving the highest intensity and the edges the lowest. Therefore, achieving a more uniform LED light power density is expected to significantly increase PCE.

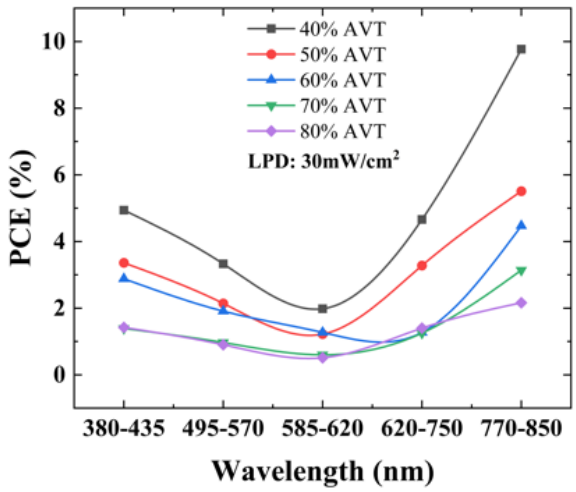



**Figure 7** PCE of the CdTe solar panels with different transparencies vs wavelength of the LEDs.

The measured PCE values of the semitransparent CdTe photovoltaic panels exhibit a clear wavelength dependence under LED illumination, with increasing PCE observed as the LED wavelength approaches approximately 850 nm, corresponding closely to the CdTe bandgap energy (~1.5 eV). In contrast, lower PCE values are observed in portions of the visible spectrum around 585-620 nm, where excess photon energy above the CdTe bandgap contributes to larger thermalization losses.

This behavior primarily reflects spectral matching between the narrow-band LED emission and the CdTe absorber bandgap rather than any intrinsic enhancement of photovoltaic conversion efficiency. Compared with broadband solar illumination, narrow-band near-infrared LED illumination reduces excess above-bandgap photon energy and therefore improves wavelength-specific photon utilization within the CdTe absorber.

It is also important to note that LED illumination introduces spatial non-uniformity in optical power density due to beam divergence. LEDs positioned near the photovoltaic panels produce localized irradiance distributions in which the central region receives higher optical intensity than peripheral regions. This illumination non-uniformity contributes to variations in the measured current-voltage characteristics and may partially explain fluctuations observed in the experimental curves. More spatially uniform LED illumination conditions are therefore expected to further improve the measured photovoltaic response.

### *3.3 I-V Curves of Multiple CdTe Solar Panels Under LEDs*

In indoor environments, the potential to harness photon energy using conventional photovoltaic (PV) systems is limited by both spatial constraints and reduced light intensity relative to natural sunlight. Indoor illumination levels are typically orders of magnitude lower than direct solar irradiance, which restricts the power output achievable from standard single-surface PV deployment. In addition, architectural and functional requirements within buildings impose further limitations on the installation of large or visually intrusive photovoltaic systems.

Conventional photovoltaic deployment is therefore primarily based on two-dimensional (2D) solar harvesting, where energy conversion is confined to planar devices located on exposed surfaces

such as rooftops, facades, or windows. In this framework, photon absorption occurs predominantly within a single layer oriented in the X-Y plane, and energy extraction is limited to a surface-defined geometry.

To overcome these limitations, the concept of three-dimensional (3D) photon harvesting is introduced. This approach extends energy conversion into the volumetric Z-direction by employing multiple semitransparent photovoltaic layers arranged in a stacked or spatially distributed configuration. Unlike 2D systems, where light is absorbed at a single interface, 3D architectures enable progressive transmission and partial energy extraction across successive layers. This creates a depth-dependent photon utilization pathway, allowing the same incident light field to be harvested multiple times as it propagates through the structure. In this sense, 3D harvesting refers to the utilization of interior volume rather than surface-only collection.

Transparent and semitransparent solar panels can be integrated into windows, walls, ceilings, and other architectural elements, enabling energy generation without significantly compromising building aesthetics or functionality [8, 9]. For example, stacked or layered PV structures may be implemented as suspended ceiling systems installed between rows of LED lighting, thereby interacting directly with indoor artificial light fields.

To investigate this concept experimentally, we designed two representative configurations. The first is shown in Figure 8, where five CdTe PV panels are arranged in a parallel stacked geometry with four infrared LEDs surrounding the system. As illustrated, the semitransparent CdTe layers are spaced at controlled distances, enabling controlled light transmission and sequential energy harvesting across multiple layers. By maintaining an average visible transmittance (AVT) between 40% and 80%, a substantial fraction of incident LED light can be progressively utilized by successive PV layers for cumulative electricity generation. This configuration enables distributed energy harvesting across the interior volume of the system, thereby demonstrating the practical implementation of volumetric (3D) indoor photon harvesting.

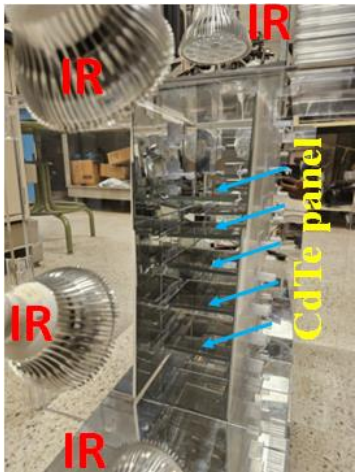



**Figure 8** The experimental setup for the I-V curve measurements of multiple CdTe panels.

In this setup, the combined electricity output from multiple solar panels surpasses that of a single layer, resulting in a notable increase in total power generation. In this study, we conducted I-V curve measurements on five commercial CdTe solar panels with varying transparencies: 40%, 50%, 60%, 70%, and 80%. These CdTe solar panels were stacked in parallel with decreasing transparency (i.e., the 80% PV is positioned on the top). Three IR lights (86 W) are situated in the front and one on top

of the PV stack, as illustrated in Figure 8. The distances between the IR bulbs and each PV panel are adjusted to maintain a light power density of 25 mW/cm$^2$ on each PV panel. The maximum output power, power conversion efficiency (PCE), and other PV parameters are computed based on the I-V curve data and listed in Table 7 and Table 8. This stacking arrangement ensures that each lay-er contributes to the overall energy output, effectively utilizing the available light.

**Table 7** The I-V curve parameters of multiple CdTe solar panels in ascending order.

| Solar Panel AVT | $V_{OC}$ (V) | $I_{SC}$ (A) | $P_{MAX}$ (W) | FF | PCE | Light Power Density (mW/cm$^2$) |
|---|---|---|---|---|---|---|
| 40% | 12.682 | 0.079 | 0.512 | 0.511 | 9.1% | 25 |
| 50% | 11.329 | 0.043 | 0.195 | 0.400 | 3.5% | 25 |
| 60% | 11.945 | 0.025 | 0.150 | 0.502 | 2.7% | 25 |
| 70% | 10.201 | 0.014 | 0.069 | 0.483 | 1.2% | 25 |
| 80% | 11.302 | 0.018 | 0.065 | 0.319 | 1.1% | 25 |

**Table 8** The I-V curve parameters of multiple CdTe solar panels in descending order.

| Solar Panel AVT | $V_{OC}$ (V) | $I_{SC}$ (A) | $P_{MAX}$ (W) | FF | PCE | Light Power Density (mW/cm$^2$) |
|---|---|---|---|---|---|---|
| 80% | 0.031 | 11.045 | 0.157 | 0.458 | 2.8% | 25 |
| 70% | 0.026 | 11.522 | 0.085 | 0.283 | 1.5% | 25 |
| 60% | 0.011 | 9.324 | 0.050 | 0.487 | 0.9% | 25 |
| 50% | 0.012 | 10.977 | 0.076 | 0.576 | 1.4% | 25 |
| 40% | 0.029 | 11.880 | 0.184 | 0.534 | 3.3% | 25 |

For the multi - panel experiments, we selected the IR LED with a wavelength range of 770 nm to 850 nm. The I-V curves obtained in ascending (Figure 9a) and descending (Figure 9b) orders are depicted in Figure 9. As illustrated in Figure 9a, the I-V curves align with the AVTs of the PV panels, with the 40% panel exhibiting the highest $I_{SC}$ as it is placed on the very top (Figure 9a). Subsequently, $I_{SC}$ decreases in accordance with both AVT and the number of panels, with the 40% AVT panel positioned at the top, followed by the 50% panel, the 60% panel, the 70% panel, and finally the 80% panel at the bottom. Despite the decrease in both $I_{SC}$ and output power at the lower panels, all panels demonstrate appreciable output power as shown in Table 7.

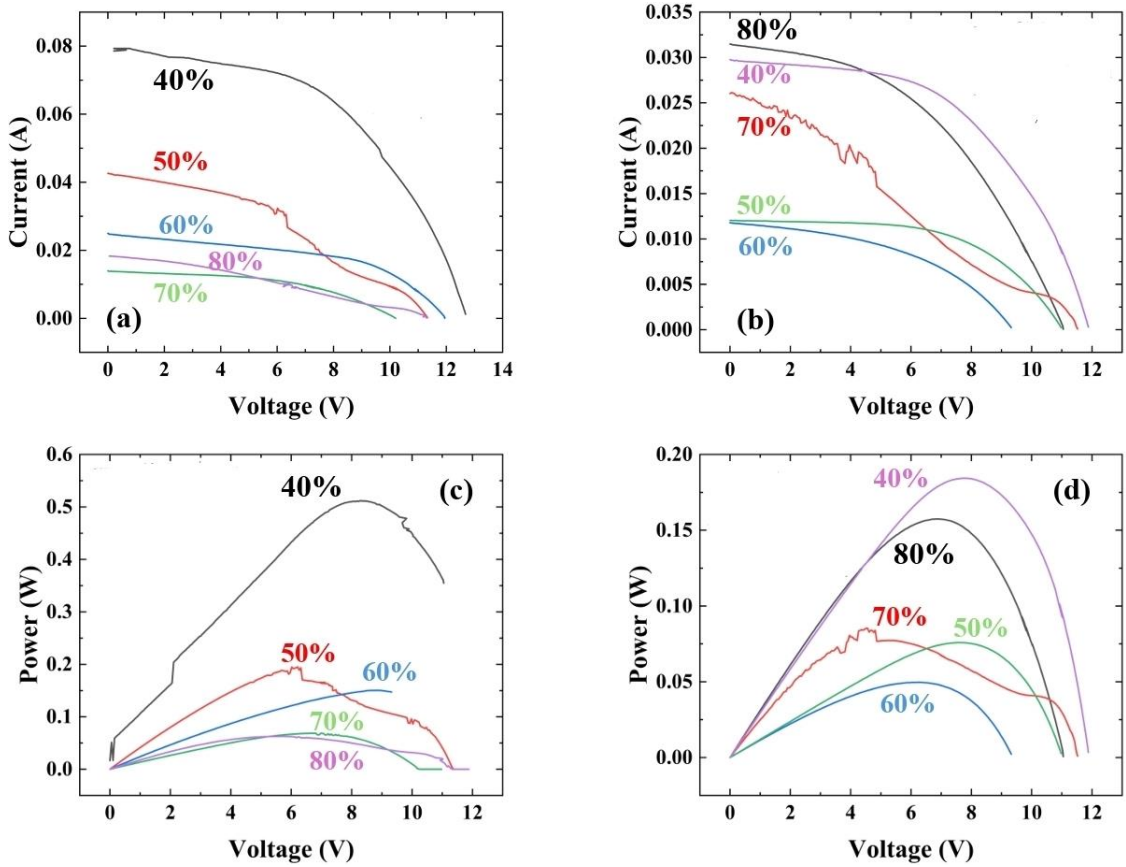



**Figure 9** I-V curves of CdTe solar panels with different transparencies that are arranged in (a) ascending and (b) descending order. Output powers of CdTe solar panels with different transparencies that are arranged in (c) ascending and (d) descending order.

Figure 9b illustrates the I-V curves for the multi - panels arranged in descending or-der. Interestingly, although the 80% panel is placed on the very top, its $I_{SC}$ is comparable to that of the 40% panel indicating substantial photon harvesting even at the bottom due to high transparencies of the panels above it. Consistently, the $I_{SC}$ values of the 70%, 60%, and 50% panels are in accordance with their positions in the stack. The output powers of CdTe solar panels with different transparencies are shown in Figures 9c (ascending order) and 9d (descending order). These parameters are summarized in Table 7 and Table 8, based on the I-V measurements presented in Figure 9.

The I-V curve parameters of multiple CdTe solar panels in ascending order are presented in Table 7. In this arrangement, light power density attenuates from the top PV (40%) to the bottom one (80%). However, each PV panel demonstrates commendable maximum power output ($P_{MAX}$) under a constant light source (25 mW/cm$^2$). While the $P_{MAX}$ of individual panels may be somewhat limited, the combined output power from all five panels significantly exceeds that of a single panel. For instance, using only a single PV with 40% average visible transmittance (AVT), the $P_{MAX}$ is 0.512 W (with our experimentally measured maximum single-layer PCE reaching 9.8%, indicating that single-junction configurations face practical efficiency ceilings near this threshold under standard operating conditions). When combined with four more PVs added in the ascending order configuration, the $P_{MAX}$ increases to 0.991 W, representing a 93% increase compared to a single 40% AVT panel. In the descending order configuration (Table 8), with an 80% AVT panel on top, the $P_{MAX}$

increases from 0.157 W to 0.552 W, corresponding to a 252% increase in $P_{MAX}$ compared to a single 80% AVT panel. With optimized design and configuration, this output power can be further enhanced.

The PCE values are also increased with multiple PV panels. In ascending order, the top 40% panel exhibits the highest PCE of 9.1%, with PCEs of subsequent panels decreasing notably due to reduced light power densities. However, upon calculating the PCE of the entire system comprising all five solar panels, the multi - panel system yields an im-pressive PCE of 17.6%. This scenario underscores that by stacking five solar panels together, we can elevate the PCE from 9.1% to 17.6%, marking a remarkable 93% increase through multiple layers - an exceptional advancement. For descending order as shown in Table 8, the PCE of the single panel of 80% on the top is 2.8%. Adding all five panels together results in a total system PCE of 9.9%. Therefore, the total increase in PCE is 253%.

It should be noted that the higher relative power conversion efficiency observed under specific indoor LED spectra represents a normalized efficiency comparison based on incident photon flux and spectral matching, rather than an absolute power output exceeding outdoor solar conditions or violating fundamental thermodynamic limits.

The second type of experimental set up is schematically shown in Figure 10a with five CdTe solar panels arranged in a stack. Similarly, these PVs are also arranged with AVT values in either descending or ascending order (Figure 10b). In this way, the LED light can penetrate all PVs, resulting in 3D photon harvesting through multiple PVs. For consistency, we chose to position one LED (585 nm-620 nm) on the top and adjusted the distance between the top PV and LED for a constant light power density of 30 mW/cm$^2$ on the top PV surface. Expectedly, the light power density decreases at each PV beneath the top one due to photon absorptions at each PV panel.

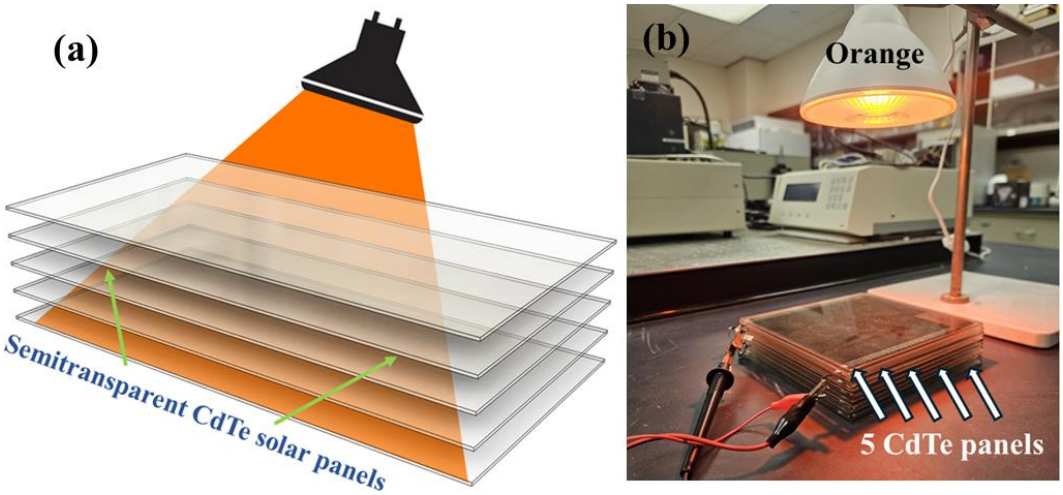



**Figure 10** (a) Schematic diagram showing 3D light harvesting through multiple semitransparent CdTe PV panels. (b) Experimental set up with a single orange LED (585 nm-620 nm) on the top and 5 CdTe PV panels arranged in a stack. The AVT values of the the PV panels are arranged in either descending or ascending order.

The I-V curves and output powers obtained are presented in Figure 11. Figure 11a shows that the I-V curves align with the light power densities on each solar panel, ordered by the AVTs of the PVs in ascending order (with the 40% panel on top). The 40% panel, having the highest PCE (7.8%) and receiving the maximum light power density of 30 mW/cm$^2$, achieves a $P_{MAX}$ of 0.531W (Table 9).

However, due to the lower transparency of the 40% panel, the light power densities are greatly reduced, leading to a sharp decrease in $I_{SC}$ values for all panels beneath it, as shown in Table 9. Conversely, when the 80% AVT PV is placed on top, each panel underneath generates a substantial $I_{SC}$, as seen in Figure 11b. Table 10 shows that with the higher AVT of 80% on top, the light power densities are significantly greater compared to those arranged in ascending order (Table 9). As a result, the $P_{MAX}$ values decline more steeply for the ascending order arrangement (Figure 11c) and more gradually for the descending order (Figure 11d).

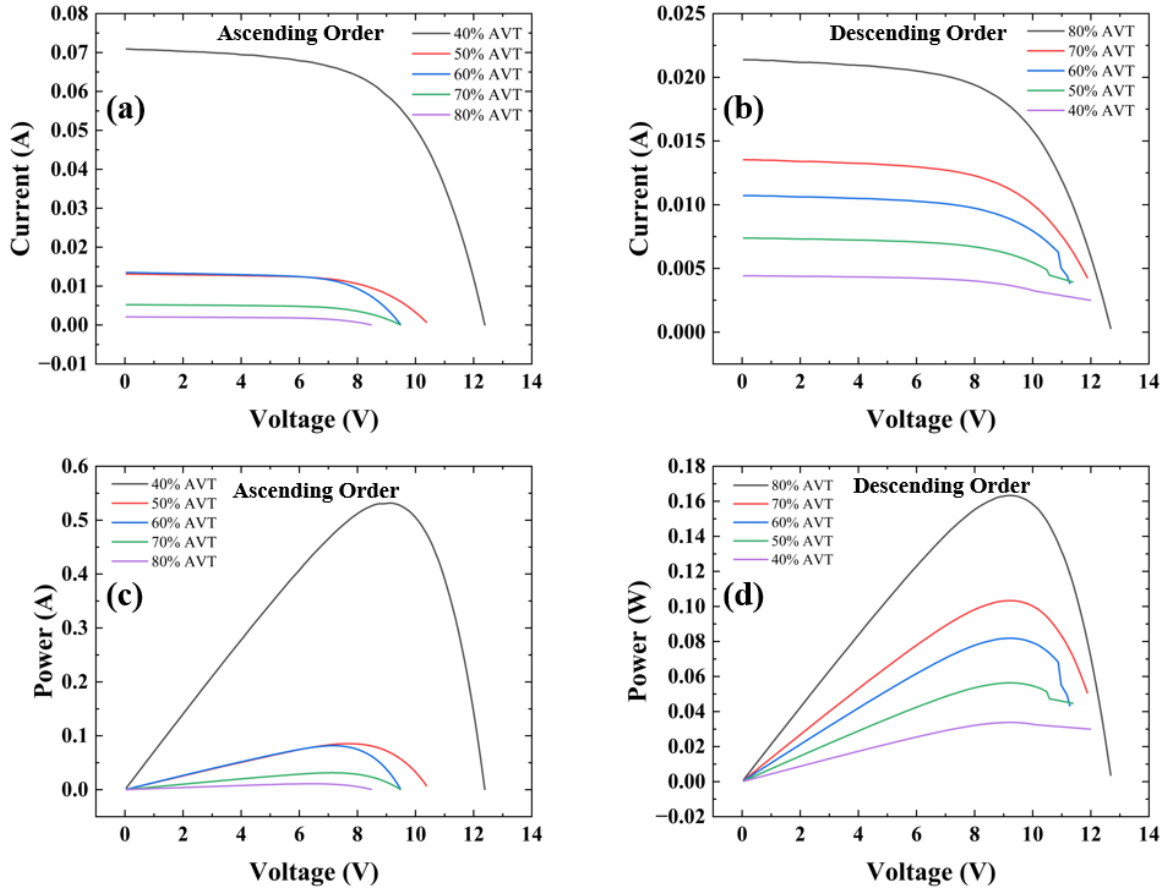



**Figure 11** I-V curves of CdTe solar panels with different transparencies that are arranged in (a) ascending and (b) descending order. Output powers of CdTe solar panels with different transparencies that are arranged in (c) ascending and (d) descending order.

**Table 9** The I-V curve parameters of a stack of multiple CdTe solar panels in ascending order.

| Solar Panel AVT | $V_{OC}$ (V) | $I_{SC}$ (A) | $P_{MAX}$ (W) | FF | PCE | Light Power Density (mW/cm$^2$) |
|---|---|---|---|---|---|---|
| 40% | 12.68 | 0.050 | 0.531 | 0.837 | 7.8% | 30.00 |
| 50% | 10.37 | 0.047 | 0.085 | 0.174 | 3.1% | 12.00 |
| 60% | 9.47 | 0.049 | 0.051 | 0.174 | 3.8% | 6.00 |
| 70% | 9.58 | 0.045 | 0.031 | 0.071 | 3.8% | 3.60 |
| 80% | 8.46 | 0.042 | 0.011 | 0.030 | 1.9% | 2.52 |

**Table 10** The I-V curve parameters of a stack of multiple CdTe solar panels in descending order.

| Solar Panel AVT | $V_{OC}$ (V) | $I_{SC}$ (A) | $P_{MAX}$ (W) | FF | PCE | Light Power Density (mW/cm$^2$) |
|---|---|---|---|---|---|---|
| 80% | 12.38 | 0.021 | 0.163 | 0.627 | 2.4% | 30.00 |
| 70% | 11.88 | 0.013 | 0.103 | 0.667 | 1.9% | 24.00 |
| 60% | 11.27 | 0.010 | 0.082 | 0.727 | 2.2% | 16.80 |
| 50% | 11.38 | 0.007 | 0.056 | 0.702 | 2.3% | 10.80 |
| 40% | 11.98 | 0.004 | 0.034 | 0.709 | 3% | 5.04 |

To further elucidate the role of layer ordering in multilayer indoor PV systems, both ascending and descending average visible transmittance (AVT) configurations were investigated. In the ascending AVT arrangement, less transparent (lower-AVT) CdTe layers are placed closer to the incident light source, with progressively more transparent layers positioned below. This configuration favors early-stage photon absorption, allowing the upper layers to harvest a larger fraction of the incident light and resulting in higher cumulative electrical output (reaching a total PCE of 20.51% compared to 7.86% for a single 40% AVT panel, as shown in Figure 12a). In contrast, the descending AVT configuration places the more transparent layers on top and the less transparent layers at the bottom, permitting a greater portion of the incident light to propagate through the entire stack. While this arrangement may yield a lower total electrical output (achieving a total PCE of 11.76% compared to 2.41% for a single 80% AVT panel, as illustrated in Figure 12b), it preserves downstream light transmission, which can be advantageous for interior illumination, visual comfort, and architectural transparency. Although optical losses such as interlayer scattering and reflection were not explicitly modeled, comparing these two stacking orders enables a practical assessment of the trade-offs between maximizing energy generation and maintaining light delivery. This comparison demonstrates that AVT sequencing provides an additional design parameter for tailoring multilayer indoor PV systems to application-specific priorities, such as energy harvesting versus daylighting or aesthetic considerations.

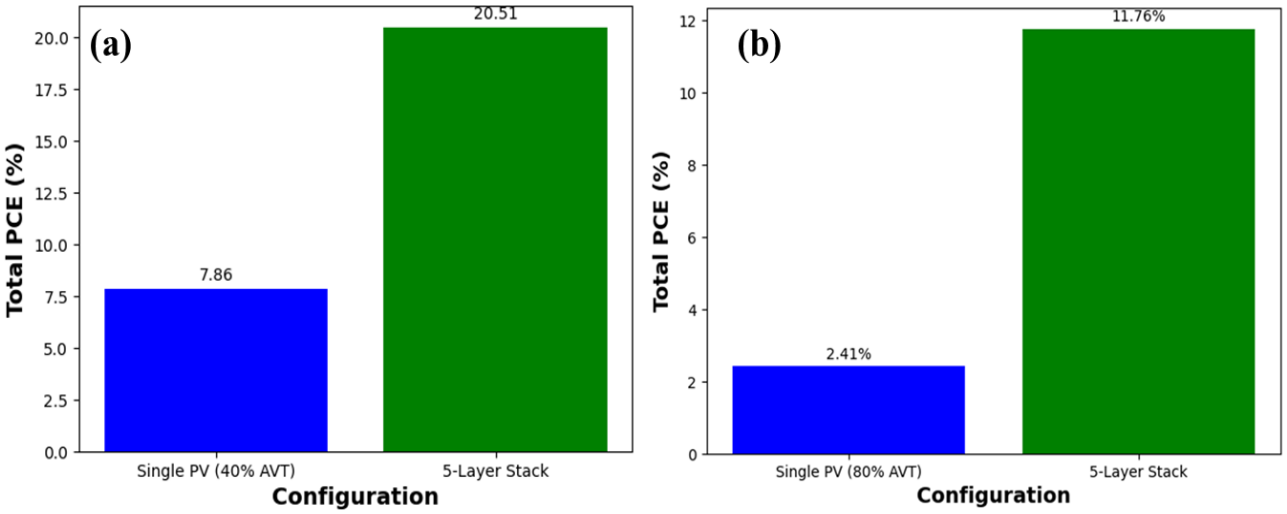



**Figure 12** Comparison of total PCE between single PV of 40% AVT vs 5-layer stack.

The multilayer semitransparent photovoltaic configuration investigated in this study is not intended to increase the intrinsic thermodynamic conversion efficiency beyond the available incident optical energy. Rather, the objective is to experimentally investigate sequential photon transmission, partial absorption, and distributed optical-energy recovery across multiple semitransparent photovoltaic layers integrated within illuminated indoor environments.

In multilayer semitransparent photovoltaic systems, incident photons that are not absorbed by upper layers can remain partially available to downstream layers through sequential optical transmission. As a result, multilayer stacking redistributes photon absorption spatially throughout the structure rather than generating additional energy or increasing the intrinsic efficiency limit of the photovoltaic material itself.

Unlike tandem photovoltaic systems designed for spectral splitting using multiple absorber bandgaps, the present same-bandgap multilayer configuration serves primarily as a proof-of-concept architecture for investigating photon-utilization behavior under indoor LED illumination conditions. Because each semitransparent layer transmits a portion of the incident optical field, successive layers remain capable of partial photon harvesting while simultaneously preserving visible-light transmission and architectural transparency.

Accordingly, the observed increase in cumulative electrical output reflects distributed photon utilization across multiple semitransparent surfaces under a fixed incident optical-energy input rather than a violation of energy-conservation principles. Similar multilayer photon-utilization behavior was previously observed in our earlier study involving stacked semitransparent CdTe photovoltaic architectures [21]. Future studies may further improve photon utilization through mixed-bandgap semitransparent photovoltaic systems, wavelength-selective optical structures, spectral-management strategies, or hybrid transparent photovoltaic architectures.

## 4. Discussion

### *4.1 Spectral Matching and Wavelength-Dependent Photovoltaic Response*

Figure 5, Figure 6, Figure 7, Figure 9, and Tables 1-8 collectively demonstrate the strong performance of semitransparent CdTe photovoltaic (PV) cells in converting diffused LED light into electricity. Notably, the 40% AVT CdTe panel achieved a higher power conversion efficiency (PCE) under LED lighting than under natural sunlight, despite operating at a lower light power density (30 mW/cm$^2$). This highlights the potential of CdTe PVs for indoor energy harvesting. Unlike sunlight, which provides uniform and broad - spectrum illumination, LED light is both spectrally narrow and spatially divergent [29]. This divergence leads to non - uniform light distribution across the PV surface, a characteristic of diffused light. However, when the LED emission spectrum aligns closely with the CdTe bandgap (~1.5 eV or 826 nm), efficiency can be significantly enhanced. The mean photon energy ($\bar{E}_{photon}$) for each LED emission band is calculated using the Planck-Einstein relation: $\bar{E}_{photon} = hc/\bar{\lambda}$, where $h$ is Planck's constant, $c$ is the speed of light, and $\bar{\lambda}$ is the midpoint wavelength of the respective spectral band. The bandgap-utilization factor ($\eta_{\text{util}}$) is subsequently defined as the ratio of the semiconductor bandgap ($E_g$ = 1.5 eV for CdTe) to the mean photon energy: $\eta_{util} = E_g/\bar{E}_{photon}$.

It is important to clarify that the higher power conversion efficiency (PCE) observed under near-infrared (IR) LED illumination compared to natural sunlight does not imply that indoor artificial lighting is superior to sunlight for absolute energy generation. This variation stems from two distinct

factors: first, the lower incident power density of the LED setup (30 mW/cm$^2$) compared to natural sunlight (55.4 mW/cm$^2$); and second, the fundamental spectral matching effect where narrow-band IR illumination eliminates excess above-bandgap photons, thereby minimizing thermalization losses. When evaluated in terms of absolute power output rather than normalized PCE, the 40% AVT CdTe panel yields a maximum power ($P_{MAX}$) of 1.072 W under natural sunlight (55.4 mW/cm$^2$), compared to 0.660 W under IR LED illumination (30 mW/cm$^2$). Thus, while narrow-band indoor lighting provides favorable spectral utilization for specific bandgaps, solar irradiation delivers substantially higher absolute power generation capacity.

These results support the feasibility of using diffused LED light for PV electricity generation. They also emphasize the importance of spectral matching between light sources and PV materials. As shown by Shockley and Queisser [29], traditional solar cells suffer from spectral losses due to mismatches between photon energy and the semiconductor bandgap. The Shockley - Queisser (SQ) limit, which accounts for blackbody radiation, recombination, and spectral losses, caps silicon PV efficiency at ~35% [30-33]. Spectral losses occur when photons have energies either below the bandgap (sub - bandgap absorption) or far above it (thermalization losses). High - energy photons excite electrons to higher states, but excess energy is quickly lost as heat, reducing overall efficiency. The spectral response of CdTe PVs (Figure 13) is negligible below 400 nm, peaks near 830 nm, and drops sharply beyond that [34, 35]. Our results (Figure 7) show that PCE follows this spectral response, with moderate efficiency in the UV, a dip in the visible range, and a rise near the bandgap. The 40% AVT panel shows a more pronounced increase in PCE compared to the 80% AVT panel.

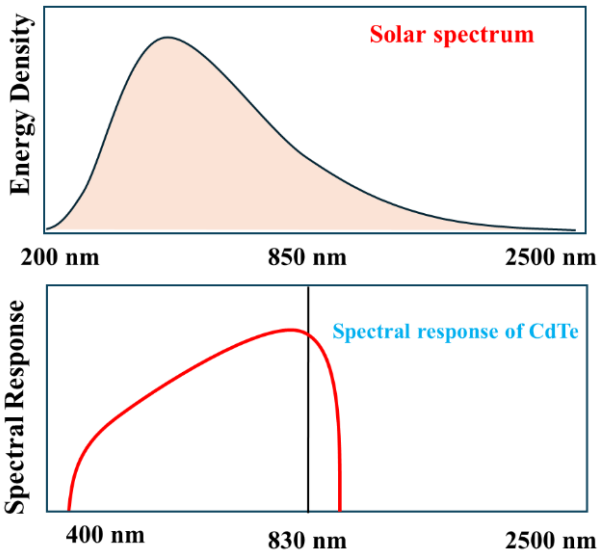



**Figure 13** Schematic diagrams of solar spectrum (top) and spectral response of CdTe PV cells (bottom).

These findings provide the base for the selection of indoor LED lighting tailored to specific PV materials [36]. LEDs can serve dual purposes: providing illumination and powering PVs. Our data confirm that LEDs emitting in the visible and near - infrared ranges can generate substantial PV output. However, the semi - transparent CdTe panels used here may not reach optimal PCE under standard LED spectra. For example, a single - layer CdTe panel with 40% AVT is unlikely to exceed 10% PCE. CdTe was chosen for its availability, but other technologies - such as dye - sensitized solar cells (DSSC), silicon, and perovskites - may offer higher efficiencies under indoor lighting. These

alternatives, when paired with optimized LED sources, could enhance electricity generation on interior surfaces.

A first-order spectral mismatch metric was employed to quantify how well the LED emission bands align with the CdTe absorber bandgap. Specifically, we defined a bandgap-utilization factor as the ratio of the CdTe bandgap energy to the mean photon energy of the illumination band, corresponding to the representative LED wavelength range. This factor estimates the maximum fraction of incident photon energy that could, in principle, be converted into useful electrical energy in a single-junction device, with the remainder lost to thermalization. The associated thermalization loss fraction is simply the complement of this ratio. A bandgap-utilization factor closer to unity indicates better spectral matching and lower excess photon-energy loss, whereas smaller values signify greater mismatch and higher thermalization losses. This metric provides a straightforward quantitative basis for comparing wavelength-dependent energy utilization trends across the different LED bands investigated in this study.

The bandgap-utilization factor and thermalization loss fraction presented in Table 11 were calculated using a first-order metric based on the midpoint wavelength ($\bar{\lambda}$) of each LED emission band. The mean photon energy ($\bar{E}_{photon}$) was determined from the band midpoint using the Planck-Einstein relation ($\bar{E}_{photon} = hc/\bar{\lambda}$). The bandgap-utilization factor was subsequently defined as the ratio $E_g/\bar{E}_{photon}$, where $E_g$ = 1.5 eV represents the CdTe bandgap, and the thermalization loss fraction was calculated as its complement ($1 - E_g/\bar{E}_{photon}$). While this first-order metric provides a transparent baseline for comparing upper-bound energetic limits across wavelength bands, it represents a simplifying approximation that does not account for wavelength-dependent variations in the CdTe absorption coefficient or internal quantum efficiency (EQE).

**Table 11** First-order spectral mismatch for semitransparent CdTe under LED illumination, using the bandgap-utilization factor and corresponding thermalization loss fraction.

| LED band | Range (nm) | Midpoint $\bar{\lambda}$ (nm) | eV | Bandgap Utilization Factor | Thermalization Fraction |
|---|---|---|---|---|---|
| Purple | 380-435 | 407.5 | 3.043 | 0.493 | 0.507 |
| Green | 495-570 | 532.5 | 2.329 | 0.644 | 0.356 |
| Orange | 585-620 | 602.5 | 2.058 | 0.729 | 0.271 |
| Red | 630-750 | 690.0 | 1.797 | 0.835 | 0.165 |
| IR | 770-850 | 810.0 | 1.531 | 0.980 | 0.020 |

The quantification in Table 11 shows that the IR band (770-850 nm) is the closest match to the CdTe bandgap, with the lowest above-bandgap energy loss, consistent with the experimentally observed increase in PCE as the illumination wavelength approaches ~850 nm. The increase in measured PCE under near-infrared LED illumination is primarily attributed to improved spectral matching between the LED emission band and the CdTe absorber bandgap (~1.5 eV), rather than enhanced intrinsic energy conversion capability. Because PCE is normalized to the incident optical power, narrow-band illumination with photon energies closer to the absorber bandgap can reduce thermalization losses and increase the fraction of incident photon energy that is theoretically convertible into electrical energy.

To quantify this effect, a first-order spectral mismatch metric based on a bandgap-utilization factor was introduced. The analysis shows that the infrared LED band exhibits the closest spectral alignment with CdTe, resulting in lower excess photon-energy loss and improved bandgap utilization efficiency compared with shorter-wavelength illumination. Accordingly, the observed PCE enhancement should be interpreted as a wavelength-dependent photovoltaic response under spectrally selective illumination rather than evidence of superior overall energy generation performance relative to broadband solar irradiation.

In multilayer semitransparent photovoltaic systems, incident photons not absorbed by upper layers can remain partially available to subsequent downstream layers. As a result, multilayer stacking redistributes photon absorption spatially throughout the structure rather than increasing the intrinsic conversion efficiency of the photovoltaic material itself. The total electrical output of the multilayer system therefore arises from sequential partial absorption and transmission processes across multiple semitransparent photovoltaic layers.

Accordingly, the cumulative multilayer response should be interpreted as enhanced photon utilization within a fixed incident optical-energy input rather than creation of additional energy or violation of thermodynamic constraints. The performance metric of the multilayer structure is therefore defined relative to the total incident optical power entering the system.

Similar multilayer photon-utilization behavior was previously observed in our earlier study on stacked semitransparent CdTe photovoltaic architectures [21], where sequential transmission through multiple semitransparent layers produced enhanced cumulative electrical output relative to individual single-layer devices under identical illumination conditions.

The multilayer semitransparent photovoltaic configuration demonstrated enhanced cumulative photon utilization compared with single-layer photovoltaic configurations under the investigated illumination conditions. The measurements presented in Figures 8-11 and Tables 7-10 reveal that each semitransparent CdTe PV panel demonstrates commendable PCE under a constant light source [21, 37-42]. While the PCE of individual panels may be somewhat limited, the combined output from all five panels surpasses that of a single panel.

Using two different experimental setups, as shown in Figure 8 and Figure 10, both yielded significant increases in PCE and power output. In the setup depicted in Figure 8, where LED lights are directed from various incident angles, the topmost panel, which receives the most intense LED radiation, achieves the highest PCE of 9.14%. The PCE of each subsequent panel decreases due to reduced light power densities. However, when calculating the PCE of the entire system comprising all five solar panels, the multi - panel system achieves an impressive PCE of 17.6%. This demonstrates that arranging five solar panels in parallel with equal spacing can elevate the PCE from 9.1% to 17.6%, marking a remarkable 93% increase through multiple layers - a significant advancement. In the descending order configuration, as shown in Table 8, the PCE of the single 80% panel on top is 2.8%. When all five panels are combined, the total system PCE reaches 9.9%, resulting in a total increase of 253%. These findings highlight the substantial multi - layer stacking in enhancing the overall efficiency of PV systems.

### *4.2 Multilayer Optical Modeling and Architectural Integration Considerations*

Figure 10 illustrates an alternative light-harvesting design using a stack of CdTe panels under a single IR LED, offering a more space-efficient configuration. Similar trends are observed, with PCE

increasing from 7.8% to 20.4% in the ascending order and from 2.4% to 11.8% in the descending order. The observed efficiency gains in multi-layer configurations arise from photon utilization rather than intrinsic improvements in the photovoltaic conversion of individual CdTe modules. In a semitransparent device, a substantial fraction of incident light is transmitted rather than absorbed. Stacking these layers converts the transmitted photons from upstream panels into usable illumination for downstream panels, effectively harvesting energy that would otherwise leave the system.

We clarify that system-level power conversion efficiency (PCE) is defined strictly by the total optical input power incident across the active areas. For multi-source configurations (Figure 8) involving side-and-top LED arrangements, system input power includes the aggregate optical power from all individual LED sources impinging on the respective panels. For single-source top-down stacked configurations (Figure 10), input power is referenced to the top surface, accounting for sequential transmission.

In a first-order optical model, each panel $i$ is treated as a spectral selective element with transmittance $T_i(\lambda)$, reflectance $R_i(\lambda)$, and absorptance $A_i(\lambda) = 1 - T_i(\lambda) - R_i(\lambda)$. Neglecting inter-layer reflections, the spectral irradiance reaching panel $i$ is given by

$$I_{SC}(n) = I_{SC}(1) \cdot \prod_{i=1}^{n-1} (1 - T_i) \quad (1)$$

where $I_0(\lambda)$ is the incident irradiance on the first layer. This framework explains why deeper layers exhibit lower local PCE ($PEC_i = P_{out,i}/P_{in,i}$) due to reduced irradiance, yet their outputs remain additive, increasing the system-level PCE defined as

$$\eta_{sys}(n) = \sum_{j=1}^{n} PCE_j \cdot \left(\frac{I_{inc,j}}{I_{total}}\right) \quad (2)$$

where $T_{j,eff}$ is the source-weighted transmittance of layer $j$ under the LED spectrum. Accordingly, the system-level efficiency reflects the combined contribution of all layers through photon cascading. This formulation also provides a physical rationale for comparing ascending versus descending AVT configurations: ascending AVT stacks maintain higher transmitted irradiance to downstream layers, maximizing electrical recovery, while descending AVT arrangements prioritize light transmission for interior illumination at the expense of reduced system-level power output.

Harvesting indoor lights presents significant economic advantages over the outdoor PV installations that incur additional expenses such as structural support, weatherproofing, solar tracking actuators. Indoor PV systems can be retrofitted within the existing infrastructure in the vicinity of the LED lights - as a reliable photon source. This approach minimizes installation complexities and associated costs. While initial panel costs may not differ substantially, the long - term cost - effectiveness of indoor PVs surpasses outdoor installations due to reduced maintenance, longer equipment lifespan in controlled environments, and the ability to generate electricity from existing indoor lights. Furthermore, the new concept of “photon recycling” aims to explore the possibility of generating electricity by harvesting the “wasted” indoor lights that remain lit at night in high - rises and public buildings, particularly in densely populated modern cities. Our experimental results indicate that it is highly feasible to utilize indoor light for electricity generation, which can, to a certain extent, offset the total energy consumption, while most electronic devices are passive

energy consumers. This integration enhances the economic viability and sustainability of indoor PV installations, aligning them with modern energy - neutral building designs.

Most indoor photovoltaic studies reported in the literature primarily focus on low-power energy harvesting for sensors, wearable electronics, or IoT applications operating under low-intensity ambient illumination. In contrast, the present work investigates semitransparent multilayer CdTe photovoltaic architectures designed for distributed photon utilization within illuminated architectural environments. The use of semitransparent photovoltaic layers enables simultaneous optical transmission and photovoltaic conversion, thereby allowing potential integration into interior building elements such as windows, suspended lighting assemblies, transparent partitions, and illuminated architectural structures.

The LED irradiance levels employed in the present experiments are higher than those typically encountered under uniformly distributed ambient indoor lighting conditions. However, the experimental configuration is intended to represent localized near-source illumination environments in which semitransparent photovoltaic layers are positioned in close proximity to LED lighting systems. Because optical power density decreases strongly with distance from the illumination source, substantially higher local irradiance levels can be achieved near integrated lighting structures such as suspended luminaires, illuminated architectural panels, ceiling systems, or transparent lighting assemblies.

To the best of our knowledge, this study represents one of the first experimental investigations of multilayer semitransparent CdTe photovoltaic systems under such controlled indoor illumination conditions. The objective is not to establish a finalized building-scale implementation, but rather to provide an initial proof-of-concept framework for evaluating wavelength-dependent photovoltaic response, multilayer photon utilization, and architectural integration strategies for indoor energy-harvesting applications. In this sense, the present work may serve as an experimental reference point for future studies on integrated lighting-photovoltaic systems and the design of energy-efficient built environments that incorporate distributed optical-energy recovery mechanisms.

Although CdTe photovoltaic technology offers favorable optoelectronic properties for semitransparent photovoltaic applications, environmental considerations associated with cadmium-containing materials remain important. The CdTe devices used in this study are encapsulated photovoltaic structures in which the active absorber layer is sealed between protective substrates, thereby minimizing direct environmental exposure during normal operation. Nevertheless, future large-scale implementation of semitransparent CdTe indoor photovoltaic systems would require appropriate lifecycle management, recycling strategies, and end-of-life material recovery protocols consistent with existing CdTe photovoltaic industry practices.

It should be noted that indoor light - activated PVs are intended mainly for large public buildings with a significant portion of lights remaining lit at night for security reasons. Since the lights of high - rises and public buildings remain lit at night, we assume the light operation time to be 24 hours per day, offering an additional advantage for indoor PV systems regardless of weather conditions. Below, we estimate the energy saving via indoor light - activated PVs for Willis Tower.

To address environmental concerns regarding cadmium content, commercial thin-film CdTe modules incorporate robust dual-glass encapsulation and benefit from established industrial take-back and closed-loop recycling infrastructure (such as manufacturer-led programs achieving global material recovery rates exceeding 95% for glass, laminates, and semiconductor materials), ensuring high-value resource reclamation and effective containment at end-of-life.

### *4.3 Estimated Energy Saving Via Indoor PVs for Willis Tower*

The Willis Tower case study is presented as a scenario-based order-of-magnitude analysis intended to illustrate the potential scaling behavior of indoor photovoltaic energy recovery under coupled assumptions of lighting power density, wall-plug efficiency, optical coupling, and photovoltaic conversion efficiency. It is not intended as a predictive engineering design or a detailed building energy audit.

All reported values should therefore be interpreted as bounded estimates within a defined parameter space rather than deterministic predictions of building-scale savings. In particular, the analysis explicitly reflects the energy-flow hierarchy inherent to indoor photovoltaic systems, where electrical input energy is first converted into optical energy through lighting systems before a fraction is recovered via photovoltaic conversion. Consequently, any recovered electrical output remains fundamentally constrained by the initial lighting energy input and must be interpreted as intra-system energy recovery rather than net energy generation.

To improve transparency, the calculation framework has been reorganized to explicitly separate electrical input energy, optical conversion via wall-plug efficiency, geometric coupling losses, and photovoltaic conversion efficiency. A unified sensitivity analysis is retained to reflect uncertainty in these coupled parameters. The resulting estimates therefore represent a bounded range of recoverable optical energy rather than a single deterministic value.

The economic discussion has been revised accordingly to avoid overinterpretation of absolute savings or payback periods. Any cost-related values are now presented as conditional outcomes under specified assumptions, rather than as projections of guaranteed system performance.

Willis Tower in Chicago, USA, was selected as a representative large-scale commercial building because of its substantial floor area (~418,000 $m^2$) and continuous indoor lighting demand. The purpose of this analysis is not to provide a definitive building energy simulation, but rather to illustrate the potential scalability of indoor photovoltaic integration under realistic indoor illumination conditions. The calculations are intended to establish an order-of-magnitude estimate for recoverable indoor optical energy using semitransparent photovoltaic systems integrated into interior architectural surfaces.

To ensure consistency across the manuscript, the techno-economic analysis in Section 4 and the Abstract have been harmonized around a single primary scenario (20 W/$m^2$ LED power density, 30% panel coverage, 15% PV efficiency, and $0.10/kWh electricity cost), yielding uniform annual savings of $0.81 million. The detailed input parameters and calculated metrics are summarized below.

- Total Floor Area: 418,000 $m^2$
- PV Deployment Area (30%): 125,400 $m^2$
- LED Lighting Power Density: 20 W/$m^2$
- Annual Operating Hours: 8,640 h/year
- PV Conversion Efficiency: 15%
- Annual Electricity Generation: ~8.13 GWh/year
- Projected Annual Savings: $812,880

The following calculations should therefore be interpreted as scenario-based proof-of-concept estimates rather than comprehensive building energy audits. Because indoor lighting is electrically powered, any recovered PV output represents partial recapture of emitted optical energy rather than net energy generation. A complete electrical-to-electrical energy analysis - including LED wall-

plug efficiency, lighting controls, occupant-driven operation, optical coupling losses, and power distribution losses - would be required to determine the true net energy savings at the building scale. Accordingly, the values reported here are intended as illustrative benchmarks for evaluating the feasibility and scalability of indoor photon-harvesting systems.

A preliminary techno-economic assessment of indoor photovoltaic (PV) integration at Willis Tower highlights its viability as a low-barrier strategy for energy-neutral building design. By utilizing 30% of the building's 418,000 $m^2$ floor area for PV installation (125,400 $m^2$), and assuming a 15% conversion efficiency, the system could generate approximately 8.13 GWh annually - offsetting nearly 45% of the building's LED lighting energy demand and yielding annual electricity savings of $812,880. Indoor PV panels can be mounted on walls, ceilings, or floors with minimal structural intervention - akin to hanging a painting - making installation significantly more straightforward and cost-effective than outdoor systems, which often require complex mounting, weatherproofing, and ongoing maintenance. At an estimated installation cost of $50/$m^2$, the total system cost is approximately $6.27 million, resulting in a favorable payback period of just 7.7 years.

While outdoor PV systems benefit from higher irradiance, they are constrained by limited operational hours - typically 4-5 peak sun hours per day in Chicago, translating to about 1,650 hours/year when accounting for cloud cover and seasonal variation. Assuming 30% of Willis Tower's floor area (125,400 $m^2$) is used for outdoor PV, with an irradiance of 150 W/$m^2$ and 15% efficiency, the system would generate approximately 4.66 GWh/year, resulting in annual electricity savings of $465,548. With an installation cost of $200/$m^2$, the total system cost is $25.08 million, yielding a payback period of approximately 53.9 years. This highlights the trade-off between higher irradiance and limited operational time, reinforcing the potential of indoor PV systems for continuous, low-barrier energy generation in high-rise buildings.

A preliminary techno-economic assessment of indoor photovoltaic (PV) integration at Willis Tower highlights its viability as a low-barrier strategy for energy-neutral building design. Based on the harmonized parameters, the system generates approximately 8.13 GWh annually, yielding annual electricity savings of $812,880. Indoor PV panels can be mounted on interior surfaces with minimal structural intervention, making installation significantly more straightforward and cost-effective than outdoor systems. At an estimated installation cost of $50/$m^2$, the total system cost is approximately $6.27 million, resulting in a favorable payback period of just 7.7 years.

While outdoor PV systems benefit from higher irradiance, they are constrained by limited operational hours (~1,650 hours/year in Chicago). Assuming 30% of Willis Tower's floor area is used for outdoor PV with 15% efficiency, the system would generate approximately 4.66 GWh/year, resulting in annual savings of $465,548. With an installation cost of $200/$m^2$, the total system cost of $25.08 million yields a payback period of approximately 53.9 years, reinforcing the comparative advantage of continuous indoor energy recovery. Note that the Willis Tower case study is presented strictly as a scenario-based order-of-magnitude sensitivity analysis to illustrate scaling behavior under defined parameters, rather than a deterministic engineering forecast or commercial energy audit.

The concept investigated in this work is based on indoor photon recycling and optical energy recovery within continuously illuminated environments. In electrically powered buildings, a significant fraction of emitted optical energy from indoor lighting systems is dissipated without further utilization. By integrating semitransparent photovoltaic layers into interior architectural spaces, part of this photon flux can be partially recaptured and converted back into electrical energy.

In this framework, the proposed system does not constitute net energy generation, but rather a distributed optical energy recovery mechanism operating within existing lighting infrastructures. The objective is therefore not to create additional energy, but to improve indoor photon utilization through partial recovery of otherwise unused optical energy. Accordingly, the performance metric of interest is not absolute energy generation, but the fraction of input electrical energy that can be recovered through photovoltaic conversion under indoor illumination conditions.

Although the instantaneous recovery fraction is relatively limited, indoor lighting systems in commercial buildings often operate continuously for extended periods. Consequently, cumulative annual photovoltaic energy recovery can become non-negligible when integrated over long operational durations. The recoverable energy therefore depends on both instantaneous conversion efficiency and total illumination time.

Because the photovoltaic output is generated in DC form, practical implementation would require integration with building electrical infrastructures through DC bus systems, localized storage architectures, microinverters, or hybrid AC/DC energy-management systems. Detailed electrical integration analysis remains beyond the scope of the present study but represents an important direction for future building-scale implementation and optimization.

The indoor PV offers unique advantages: continuous operation, predictable lighting, integration flexibility, and potential synergies with building aesthetics and smart energy systems. These features position indoor PV as a compelling alternative for next - generation, energy - neutral building strategies - especially when driven by broader sustainability mandates and future cost optimizations.

There is significant room for improvements in both PV technology and architectural design, particularly as we anticipate future reductions in the cost of PV systems, including multi - layered and silicon - based panels. By integrating PV technology into various aspects of building design, we can push the boundaries of sustainable energy solutions, addressing both daytime and nighttime energy needs. As PV efficiency continues to improve and installation costs decrease, the viability of these systems will only increase, making energy - neutral buildings more accessible and cost - effective. This research lays the groundwork for such advancements, emphasizing the importance of continued exploration and innovation in the field of sustainable energy, with the potential for both environmental and economic benefits.

While our study demonstrates the technical feasibility of using semitransparent CdTe PV panels to harvest indoor LED lighting, we acknowledge that a comprehensive systems - level evaluation is necessary to assess the broader deployment potential. Specifically, factors such as spatial constraints, panel orientation, lighting variability, and trade - offs in placement must be considered when designing integrated PV systems for real - world environments. However, our work is focused on establishing a proof-of-concept through controlled experimental measurements. Our goal is to provide foundational data on PV behavior under indoor lighting conditions, which can serve as a starting point for future engineering studies to model and optimize indoor PV integration. We believe that this stepwise approach - beginning with baseline performance data - is essential to inform more complex architectural and techno - economic evaluations.

In addition to performance considerations, the integration of PV panels within interior spaces naturally raises questions about potential impacts on building acoustics, spatial functionality, and interior design flexibility - including visual aesthetics and color scheme adaptability. These are important issues, especially when envisioning widespread deployment in public or commercial environments. While our current study does not address these interdisciplinary challenges directly,

we recognize their significance. As such, we view this work as an initial step to stimulate further research that incorporates architectural, ergonomic, and acoustic perspectives. The use of semitransparent materials and layered configurations offers new possibilities for unobtrusive design integration, and future investigations should explore how PV installations can be optimized to coexist with dynamic interior functions.

We also acknowledge that the scalability and generalizability of indoor PV deployment require validation across diverse building types, interior layouts, and geographic locations. Our study presents results from a controlled laboratory environment designed to simulate high - efficiency indoor lighting conditions, but we recognize the need to extend these insights to real - world settings. In the revised manuscript, we will expand our discussion to consider how these findings can serve as a baseline for future investigations in various architectural contexts - including commercial buildings, high - rises, schools, and healthcare facilities - each with different lighting schedules, spatial constraints, and energy demands. Such comparative studies are essential to evaluate the robustness and adaptability of indoor PV solutions on a broader scale.

In realistic building-integrated PV (BIPV) applications, stacking multiple semitransparent CdTe layers introduces practical challenges. Each additional absorber layer increases panel thickness and mass, complicating integration into slim window or curtain-wall assemblies, and potentially affecting aesthetic acceptance. Maintenance and durability are also critical: multilayer laminates require robust edge seals, careful cleaning to remove dust or moisture between layers, and long-term encapsulation strategies, particularly since CdTe thin films have outdoor lifetimes of ~10-20 years. To address these challenges, designers can adopt modular, serviceable panel architectures that allow individual layers or sub-modules to be replaced, use selective layer activation or bypass (e.g., dynamically deactivating rear layers or integrating electrochromic elements to tune transparency), and employ flexible mounting schemes such as hinged or sliding panels to facilitate maintenance. Advanced optical engineering - including spectrally selective coatings, high-transparency conductive layers, and optimized dielectric/metal stacks - can help balance transparency against electrical output. Collectively, these strategies demonstrate that practical multilayer BIPV requires holistic integration of materials, optics, and architecture to reconcile energy yield with aesthetic and maintenance requirements.

Using the harmonized annual savings of approximately \$0.81 million per year and a deployment area of 125,400 $m^2$, the hypothetical simple payback time depends strongly on installed cost and O&M requirements. For an installed cost of \$200 per $m^2$ (total capex \$25.08 million), the payback is about 31 years without O&M, and about 45 years if annual O&M is assumed to be 1% of capex. For higher installed costs of \$500 per $m^2$ (\$62.7 million capex) and \$1,000 per $m^2$ (\$125.4 million capex), payback periods extend significantly or become impractical when factoring in annual O&M. Conversely, achieving a 10- to 20-year payback requires a total capex of roughly \$8.1 to \$16.3 million (corresponding to \$65 to \$130 per $m^2$), indicating that economic feasibility is primarily governed by low installation and maintenance costs alongside optical coupling efficiency.

While the estimated annual savings of approximately \$0.81 million appear substantial, the corresponding simple payback period is highly sensitive to capital expenditure and maintenance costs, extending from 31 to over 100 years under realistic installed cost tiers (\$200-\$1,000/$m^2$) when factoring in annual O&M. These extended payback horizons indicate that current indoor photovoltaic retrofits are not economically viable as standalone investments under standard commercial hurdles. Economic feasibility is strictly contingent upon achieving low marginal

installation costs (e.g., \$65-\$130/$m^2$) or integrating semitransparent panels into interior surfaces already scheduled for renovation. Economic feasibility is driven primarily by achievable optical coupling and the marginal installed cost of interior PV integration. Rather than specifying a single payback period, this analysis is best interpreted parametrically: a simple payback of 10-20 years would require both high optical coupling near luminaires and low marginal installation costs-such as integration into surfaces already being installed or retrofitted - combined with manageable operation and maintenance. Future work should therefore focus on identifying high-coupling locations, low-cost integration pathways, and comprehensive building energy modeling that accounts for lighting controls and occupancy-driven operation.

As an alternative, organic photovoltaics (OPV) show considerable long-term promise for indoor and semitransparent applications owing to their lightweight, flexible, and potentially lower-toxicity characteristics. Current barriers to large-scale OPV deployment include operational stability under air, light, and thermal stress, robust encapsulation, and scalable manufacturing [43, 44]. If these challenges can be addressed, OPV systems could serve as a viable substitute for CdTe in indoor and BIPV applications, particularly in contexts where aesthetics, weight, and perceived material safety are important design considerations.

## 5. Summary

We conducted systematic experiments on the I-V curves of semitransparent CdTe PV panels under both natural sunlight and LEDs spanning various wavelengths from UV to IR. The results reveal efficient PCEs of the CdTe PVs under LEDs compared to their performance under natural sunlight. This significant discovery shows the feasibility of harnessing diffused light for continuous electricity generation, independent of weather conditions. Consequently, building lights can serve as a constant photon energy source for continuous PV electricity generation, advancing the goal of achieving energy - neutral buildings.

In modern building environments, lighting systems serve not only visual and aesthetic purposes but also represent an untapped source of renewable energy. This study explores the emerging concept of utilizing indoor lighting - particularly LED systems - not solely for illumination and ambiance, but as a continuous source of photons for photovoltaic (PV) energy harvesting. By integrating semitransparent PV panels into interior surfaces, lighting can be transformed into a dual - purpose system that supports both occupant comfort and electricity generation. This multifunctional approach enhances the sustainability profile of indoor lighting, aligning it with broader goals of energy - neutral buildings and environmentally responsible design.

Our results demonstrate that LED light can be effectively harvested using a stacked configuration of semitransparent CdTe photovoltaic panels. Although individual panels exhibit relatively modest power conversion efficiencies (PCEs), the cumulative output of the multi - panel system significantly surpasses that of a single panel. In an ascending AVT (average visible transmittance) arrangement, the stack achieves a 160.94% increase in total PCE, while a descending AVT configuration yields a 387.97% improvement, relative to a single - panel setup. This study presents a novel strategy for utilizing indoor LED lighting as a viable energy source, offering a promising pathway toward energy - neutral buildings and more sustainable infrastructure. To ensure consistency across the manuscript, the percentage improvement figures for multi-layer stacking have been unified based on experimental data: for the IR LED configuration, system PCE increases by 93.4% (from 9.1% to 17.6%)

for the ascending stack and 253.6% (from 2.8% to 9.9%) for the descending stack; for the orange LED stack (Figure 10), system PCE improves by 160.94% (from 7.86% to 20.51%)

Indoor photovoltaic (PV) systems present a compelling opportunity for substantial electricity savings in large buildings like Willis Tower. By leveraging existing infrastructure, specifically continuous LED lighting, these systems efficiently convert indoor light into electrical energy. For Willis Tower, with a total floor area of 418,000 $m^2$ and 30% allocated to PV panels at 20 $W/m^2$ LED light power density, operating 24 hours/day with a 15% conversion efficiency, significant annual energy production can be achieved.

Indoor PV systems benefit from continuous photon harvesting due to the long daily operation of indoor lighting, such as LEDs, often running 12 hours or more. This enables steady energy generation day and night, improving overall electricity production. With constant light exposure, indoor PVs can achieve higher efficiency than outdoor systems, which are affected by diurnal and seasonal sunlight changes. Unlike outdoor PVs, indoor systems are not impacted by weather conditions like clouds or rain, ensuring reliable, year - round energy output and enhanced energy security. Indoor operation also protects PVs from environmental stressors, supporting stable performance over time. Installation is typically simpler, avoiding the structural changes and weatherproofing required outdoors, thus reducing upfront costs and time. Indoor PVs also need less maintenance, lowering long - term operational expenses. Overall, they support sustainability by providing clean energy without emissions or environmental disruption.

Indoor PV systems are well - suited for integration into existing urban infrastructure, supporting sustainable development by efficiently using available indoor spaces for renewable energy generation. They can be incorporated into architectural elements such as windows, facades, and roofs, providing both design flexibility and aesthetic value while generating electricity. Such integration improves space efficiency in densely populated areas and supports more effective use of urban land.

In summary, indoor PVs offer a promising approach to improving energy efficiency and reducing costs in high - rise buildings and urban centers. Their adoption not only addresses rising energy demands but also advances sustainable building practices, positioning them as key enablers of energy - neutral architecture.

The present study should be understood as an experimental investigation of semitransparent CdTe photovoltaic behavior under controlled LED illumination in multilayer configurations designed to explore distributed photon utilization within indoor lighting environments. While the underlying principles of photovoltaic energy conversion and spectral matching are well established, the specific configuration examined here - namely sequential multilayer semitransparent CdTe structures under wavelength-controlled LED illumination - provides an experimental framework for assessing photon transmission and absorption across stacked interior photovoltaic elements.

Accordingly, this work does not introduce new physical principles but rather provides systematic experimental evidence of photon utilization behavior in a multilayer indoor photovoltaic architecture. The findings are intended to inform future design considerations for integrated lighting-photovoltaic systems in built environments, where spatially distributed semitransparent devices may be deployed to enhance optical energy utilization under controlled illumination conditions.

While extensive research exists on indoor photovoltaic harvesting for low-power IoT devices or emerging organic and dye-sensitized transparent cells, the practical implementation of robust,

commercial-grade semitransparent CdTe modules under indoor lighting remains largely unexplored. This study bridges that gap by demonstrating: (i) the first systematic evaluation of semitransparent CdTe PV architectures under wide-spectrum, wavelength-selective indoor LED illumination; (ii) novel multi-panel vertical 3D photon-harvesting and parallel cascading geometries that dramatically elevate aggregate system efficiency; and (iii) a rigorous, statistics-backed techno-economic framework evaluating building-scale deployment (such as high-rise retrofitting scenarios). Unlike conventional indoor PVs optimized solely for micro-watt IoT nodes or organic films constrained by degradation, this approach provides a scalable, industrially robust pathway for architectural energy recovery and microgrid integration.

While indoor optical energy recovery mitigates temporal variations by leveraging continuous lighting schedules, it relies fundamentally on initial grid-powered electrical input and operates as a supplemental intra-system buffer rather than an independent primary source of renewable generation.

**Acknowledgments**

The authors acknowledge the support and collaboration provided by the participating institutions.

**Author Contributions**

Conceptualization, D.S.; Data curation, A.K.; Investigation, A.H., M.B., J.K., and D.S.; Project administration, D.S.; Resources, D.S. and A.H.; Supervision, D.S. All authors have read and agreed to the published version of the manuscript.

**Funding**

This work was supported by the National Science Foundation (CMMI-1953009), the Michelman Green, Clean and Sustainable Technology Research Innovation Program (F103484), and the Swiss National Science Foundation (Project No. IZSEZ0_223270, “Photothermal Coating for Energy Efficient Windows”).

**Competing Interests**

The authors declare no conflict of interest.

**Data Availability Statement**

The data supporting the findings of this study are available from the corresponding author upon reasonable request.

**AI-Assisted Technologies Statement**

To be explicit, AI-based tools were used only for basic grammar correction and language refinement, to improve the readability of the English text. They played no part in the design of the study, the collection or analysis of data, the interpretation of results, or the formulation of conclusions, all of which were carried out by the authors. We have reviewed and edited all AI-

assisted text ourselves, and we accept full responsibility for the accuracy and integrity of the manuscript.

**References**


1. Green MA, Dunlop ED, Yoshita M, Kopidakis N, Bothe K, Siefer G, et al. Solar cell efficiency tables (Version 63). Prog Photovolt Res Appl. 2024; 32: 3-13.
2. Razykov TM, Ferekides CS, Morel D, Stefanakos E, Ullal HS, Upadhyaya HM. Solar photovoltaic electricity: Current status and future prospects. Sol Energy. 2011; 85: 1580-1608.
3. Jelle BP, Breivik C, Røkenes HD. Building integrated photovoltaic products: A state-of-the-art review and future research opportunities. Sol Energy Mater Sol Cells. 2012; 100: 69-96.
4. Wagner L, Peters IM, Anctil A, Davies M, de Groot J, Wang L, et al. Actions for sustainably scalable multi-terawatt photovoltaics. Nat Rev Clean Technol. 2026; 2: 107-122.
5. Grandhi GK, Koutsourakis G, Blakesley JC, De Rossi F, Brunetti F, Öz S, et al. Promises and challenges of indoor photovoltaics. Nat Rev Clean Technol. 2025; 1: 132-147.
6. Xie L, Song W, Ge J, Tang B, Zhang X, Wu T, et al. Recent progress of organic photovoltaics for indoor energy harvesting. Nano Energy. 2021; 82: 105770.
7. Taşer A, Koyunbaba BK, Kazanasmaz T. Thermal, daylight, and energy potential of building-integrated photovoltaic (BIPV) systems: A comprehensive review of effects and developments. Sol Energy. 2023; 251: 171-196.
8. Traverse CJ, Pandey R, Barr MC, Lunt RR. Emergence of highly transparent photovoltaics for distributed applications. Nat Energy. 2017; 2: 849-860.
9. Lunt RR. Theoretical limits for visibly transparent photovoltaics. Appl Phys Lett. 2012; 101: 043902.
10. Melchor-Robles JA, Nieto-Zepeda KE, Vázquez-Barragán NE, Arreguín-Campos M, Rodríguez-Rosales K, Cruz-Gómez J, et al. Characterization of CdS/CdTe ultrathin-film solar cells with different CdS thin-film thicknesses obtained by RF sputtering. Coatings. 2024; 14: 452.
11. Montoya FG, Peña-García A, Juaidi A, Manzano-Agugliaro F. Indoor lighting techniques: An overview of evolution and new trends for energy saving. Energy Build. 2017; 140: 50-60.
12. Yun GY, Kim H, Kim JT. Effects of occupancy and lighting use patterns on lighting energy consumption. Energy Build. 2012; 46: 152-158.
13. Byun J, Hong I, Lee B, Park S. Intelligent household LED lighting system considering energy efficiency and user satisfaction. IEEE Trans Consum Electron. 2013; 59: 70-76.
14. Roisin B, Bodart M, Deneyer A, D'herdt P. Lighting energy savings in offices using different control systems and their real consumption. Energy Build. 2008; 40: 514-523.
15. Mirrahimi S, Mohamed MF, Haw LC, Ibrahim NL, Yusoff WF, Aflaki A. The effect of building envelope on the thermal comfort and energy saving for high-rise buildings in hot-humid climate. Renew Sustain Energy Rev. 2016; 53: 1508-1519.
16. Mostafavi F, Tahsildoost M, Zomorodian Z. Energy efficiency and carbon emission in high-rise buildings: A review (2005-2020). Build Environ. 2021; 206: 108329.
17. Srivishnu KS, Rajesh MN, Prasanthkumar S, Giribabu L. Photovoltaics for indoor applications: Progress, challenges and perspectives. Sol Energy. 2023; 264: 112057.
18. Yun GY, Jung H, Kim JT. Energy-saving potential of LED lighting systems. Indoor Built Environ. 2013; 22: 235-241.

19. Kıyak İ, Oral B, Topuz V. Smart indoor LED lighting design powered by hybrid renewable energy systems. Energy Build. 2017; 148: 342-347.
20. Chew I, Kalavally V, Oo NW, Parkkinen J. Design of an energy-saving controller for an intelligent LED lighting system. Energy Build. 2016; 120: 1-9.
21. Katepalli A, Wang Y, Shi D. Solar harvesting through multiple semi-transparent cadmium telluride solar panels for collective energy generation. Sol Energy. 2023; 264: 112047.
22. O'Kane M. Solar Cell Efficiency Formula [Internet]. Sheffield, UK: Ossila; 2026. Available from: https://www.ossila.com/pages/solar-cell-efficiency-formula.
23. Meddeb H, Götz-Köhler M, Neugebohrn N, Banik U, Osterthun N, Sergeev O, et al. Tunable photovoltaics: Adapting solar cell technologies to versatile applications. Adv Energy Mater. 2022; 12: 2200713.
24. Burst JM, Duenow JN, Albin DS, Colegrove E, Reese MO, Aguiar JA, et al. CdTe solar cells with open-circuit voltage breaking the 1 V barrier. Nat Energy. 2016; 1: 16015.
25. Morales-Acevedo A. Thin film CdS/CdTe solar cells: Research perspectives. Sol Energy. 2006; 80: 675-681.
26. Metin B, Kavasoglu N, Kavasoglu AS. AFORS-HET simulation for investigating the performance of ZnO/n-CdS/p-CdTe/Ag solar cell depending on CdTe acceptor concentration and temperature. Physica B Condens Matter. 2023; 649: 414504.
27. Allam Z, Boudaoud C, Bouchachia B, Soufi A. Simulation of CdTe/CdS heterostructure with graphene contact. Mater Today Proc. 2022; 51: 2152-2156.
28. Barbato M, Artegiani E, Bertoncello M, Meneghini M, Trivellin N, Mantoan E, et al. CdTe solar cells: Technology, operation and reliability. J Phys D Appl Phys. 2021; 54: 333002.
29. Shockley W, Queisskr HJ. Detailed balance limit of efficiency of *p-n* junction solar cells. J Appl Phys. 1961; 32: 510-519.
30. Lee Y, Park C, Balaji N, Lee YJ, Dao VA. High-efficiency silicon solar cells: A review. Isr J Chem. 2015; 55: 1050-1063.
31. Zhang Y, Jia X, Liu S, Zhang B, Lin K, Zhang J, et al. A review on thermalization mechanisms and prospect absorber materials for the hot carrier solar cells. Sol Energy Mater Sol Cells. 2021; 225: 111073.
32. Le Bris A, Rodiere J, Colin C, Collin S, Pelouard JL, Esteban R, et al. Hot carrier solar cells: Controlling thermalization in ultrathin devices. IEEE J Photovolt. 2012; 2: 506-511.
33. Stuckelberger M, Biron R, Wyrsch N, Haug FJ, Ballif C. Progress in solar cells from hydrogenated amorphous silicon. Renew Sustain Energy Rev. 2017; 76: 1497-1523.
34. Takeguchi K, Nakayama K, Chantana J, Kawano Y, Nishimura T, Hishikawa Y, et al. Spectral gain and loss of different-type photovoltaic modules through average photon energy of various locations in Japan. Sol Energy. 2021; 214: 1-10.
35. Daxini R, Wu Y. Review of methods to account for the solar spectral influence on photovoltaic device performance. Energy. 2024; 286: 129461.
36. Hamadani BH. Understanding photovoltaic energy losses under indoor lighting conditions. Appl Phys Lett. 2020; 117: 043904.
37. Lyu M, Lin J, Shi D. Solar desalination via multilayers of transparent photothermal $Fe_3O_4$@$Cu_{2-x}S$ thin films. Energy Technol. 2021; 9: 2100590.

38. Lyu M, Lin J, Krupczak J, Shi D. Solar harvesting through multilayer spectral selective iron oxide and porphyrin transparent thin films for photothermal energy generation. Adv Sustain Syst. 2021; 5: 2100006.
39. Lin J, Krupczak J, Shi D. Solar harvesting and energy generating building skins with photothermal-photovoltaic dual-modality based on porphyrin thin films. MRS Commun. 2022; 12: 1225-1234.
40. Lin J, Wang Y, Lyu M, Deng Z, Shi D. Transparent porphyrin-based hybrid films for spectral selective solar harvesting and energy generation. Sol Energy Mater Sol Cells. 2022; 243: 111788.
41. Lyu M, Lin J, Krupczak J, Shi D. Light angle dependence of photothermal properties in oxide and porphyrin thin films for energy-efficient window applications. MRS Commun. 2020; 10: 439-448.
42. Lin J, Lyu M, Shi D. 3D solar harvesting and energy generation via multilayers of transparent porphyrin and iron oxide thin films. Energies. 2023; 16: 3173.
43. Katepalli A, Mohankumar T, Gandharapu MS, Shrestha S, Harfmann A, Bonmarin M, et al. Photon recycling for indoor energy harvesting: Optical optimization of LED-driven silicon photovoltaic systems. J Energy Power Technol. 2025; 7: 013.
44. Lu MN, Su TS, Pylnev M, Long YS, Wu TC, Tsai MA, et al. Stepwise optimizing photovoltaic performance of dye-sensitized cells made under 50-lux dim light. Prog Photovolt Res Appl. 2021; 29: 533-545.